Comparison of AUV hull designs using CFD and preparation for towing tank testing

ULRIK FALK-PETERSEN

MARIUS FONNES MYREN

BENEDICTE HÄRDIG SØREIDE

Bachelor thesis in Marine Engineering

Bergen, Norway 2020

Høgskulen på Vestlandet

Comparison of AUV hull designs using CFD and preparation for towing tank testing

Ulrik Falk-Petersen

Marius Myren

Benedicte Härdig Søreide

Department of Mechanical- and Marine Engineering

Western Norway University of Applied Sciences

NO-5063 Bergen, Norway

Høgskulen på Vestlandet

Fakultet for Ingeniør- og Naturvitskap

Institutt for maskin- og marinfag

Inndalsveien 28

NO-5063 Bergen, Norge

Norsk tittel: Sammenligning av AUV design ved bruk av CFD og
forberedelse til forsøk i slepetank.

Author(s), student number: Ulrik Falk-Petersen, h571636

                                              Marius Myren, h571621

                                              Benedicte Härdig Søreide, h180317

Study program: Marine technology

Date: May 2020

Report number: IMM 2020-M30

Supervisor at HHVL: Gloria Stenfelt

Assigned by: HVL / Havlab

Contact person: Gloria Stenfelt

Antall filer levert digitalt: 4

Preface

This bachelor thesis is written at the Department of Mechanical and Marine Engineering at Western University of Applied Sciences (HVL) at the study program Marine Technology and is based on research done in the period of January through May 2020.

Special thanks to our supervisor Dr Gloria Stenfelt for providing feedback and support, Dr Mariusz Domagala for software support, Nafez Ardestani and Harald Moen for assistance when producing the models.

Thanks to HVL for providing adequate tools for finalizing this report.

Abstract

This report was created with the belief that the optimal drone hull has not yet been developed. With nature as inspiration, the expectation is that natural selection has the answer to increased drone lifetime and peak energy efficiency. By combining designs from the world of nautical fauna with the advancements done in the research field of low-drag drone hulls, we aim to develop the autonomous underwater vehicle of tomorrow.

Even though the results do not prove that the suggested drone design outperforms the typical teardrop-shaped designs, we hope to pave the way for future drone designs by proposing several improvements for test execution, alternate hull designs and by sharing knowledge and experience of how to create an even better performing drone in the future.

Sammendrag

Denne rapporten ble utarbeidet på bakgrunn av antakelsen om at det gunstigste skroget for undervannsdroner fortsatt ikke har blitt oppdaget. Med naturen som inspirasjon er forventningen at naturlig utvalg har svarene for å oppnå lengre batterilevetid og bedre energieffektivitet. Ved å kombinere formene funnet blant havets fauna med fremskrittene gjort innen forskning for effektivisering av droneskrog, håper vi å finne designet for morgendagens undervannsfartøy.

Til tross for at resultatene ikke ga distinkt bevis for at foreslått dronedesign var mer effektiv enn en typisk tåre-formet modell, håper vi å legge til rette for videre utvikling ved å presentere reviderte metoder for testing, irregulære skrogdesign, samt å dele kunnskap og erfaring videre for å bidra til et bedre dronedesign.

Table of contents

1. Introduction

For vehicles in a fluid, a hydrodynamic hull is required in order to accomplish a diverse scope of both civilian and military tasks. An autonomous underwater vehicle (AUV) needs an efficient design in order to minimize resistance in water as well as to meet necessary requirements for increasingly complex and challenging missions, where conservation of energy mean several miles of added operational range.

Today, several different types of vehicles are used in marine observation and detection missions at sea. The shape of the hull not only affects the structural integrity, pressure distribution and displacement of the internal structure, but also the hydrodynamic force, manoeuvrability and stability [1]. Typically, each vehicle's mission will have different hydrodynamic requirements. Hugin, developed by Kongsberg Marine in the 1980s, is an AUV with great manoeuvrability and stability and is used for mapping of the seabed [2]. In Figure 1, an illustration of Hugin is shown. Sea gliders are small, reusable vehicles that are designed to glide from the surface to a calibrated depth where it measures different fluid qualities [3]. See Figure 2 for an example of a glider. Snake robots with thrusters that can transit over long distances are flexible and may be used for maintenance and inspection [4], such as Eelume in Figure 3.

Figure 1: Hugin, Kongsberg [5].   Figure 2: Seaglider, Kongsberg [6].   Figure 3: Eelume, Equinor [7].

Traditionally, empirical formulations and model testing have been used to derive hydrodynamic forces acting on a hull, but with the rapid development of digital computers and software it is now feasible to consider computational fluid dynamics (CFD) analysis instead [8]. The total costs of computational simulations are considerably lower than the costs of model testing, but experimental data is often used to validate CFD solutions as the CFD results can vary. Most AUV studies have focused on a particular design object and calculated the resistance by CFD and/or model testing, but most findings are not easily transferable to other shapes. Despite the fact that early research (1981) in the area concluded that body drag would not change much with varying nose and tail shapes [9], most AUVs have a cylindrical shape with variations in sharp- and bluntness at both ends, as well as different lengths and hull diameters, e.g. [10], [11] and [12].

There are no standard design procedures or class rules (e.g. DNV, Lloyds Register) for AUVs, resulting in an ad hoc design process [8]. Even so, three classes of AUVs have been identified based on the hydrodynamic performance of different cross-sectional shapes, with several different subdivided species according to the shape features in longitudinal cross section: rotor, flat and irregular [1]. Most AUVs will be found under the class "rotor" with either a teardrop-shape or torpedo-shape, e.g. Hugin.

A broad review of research on propeller driven AUVs reveals a lack of studies on biologically inspired designs. Due to nature's evolution and natural selection there are many aspects of nature that can serve as an inspiration for design. The use of nature to solve engineering problems is a powerful tool for innovation and problem solving [13]. Several hydrodynamic studies on fish locomotion, propulsion, manoeuvring and skin friction have been published, e.g. [14] and [15], but no research observed has investigated the difference between biologically inspired and traditional AUV hulls.

This report aims to examine whether evolution has managed to minimize drag and resistance by constructing a shark-inspired design or if the pre-existing, popular "teardrop-shaped" hull is the most effective. Software is used to create 3D-models of the hulls and the designs are then transferred to two different versions of CFD software in order to compare resistance data. Furthermore, this report describes proper steps for confirmation of data by model testing at MarinLab, HVL.

2. Method

Energy is required to drive submerged vehicles through water. The amount of required energy depends on the resistance encountered in the water and the extent to which the energy is converted into motion energy for the vessel. The resistance of a vessel is the pulling force required to tow a vessel at a given speed in still water, and that force can be estimated using models or CFD. Thus, in this section the test objects, theoretical, numerical, and experimental approach for drag calculation are explained.

2.1 Test objects

The AUV design process usually starts with identifying mission objectives and necessary internal subsystems (e.g. batteries, etc.) [8]. However, due to lack of information and knowledge regarding required equipment dimensions the size of the test objects are based on the operating limits for the CNC machine used to create the physical models. Due to lab restrictions, the velocity interval for testing are from 0.5 m/s up to 5 m/s with an increment of 0.5 m/s.

The max production length of the CNC machine leads to an optimal drone length of just under 90 cm. This length allows the drone parts to be made in one go, instead of having to create up to 8 parts with a length of more than 90 cm. Due to the nature of the inaccuracies in the test equipment, bigger drones would yield more accurate results as small differences in water conditions can ruin test results on smaller drones. The smaller the drone, the bigger these inaccuracies are. Therefore, it was decided to find a middle ground between reducing the chance for inaccuracies, as well as making the production easier and more accurate. If the hull would prove to have better results than the baseline model, a bigger drone could be created later for more thorough testing.

In this report Creo Parametric [16] is used to create 3D-models and fluid domains for CFD analysis. The model properties are all set to millimetres. In the following sections the process of model design and properties are presented.

2.1.1   Teardrop shaped hull – reference model

The teardrop shaped hull is our reference model, and is a typical streamlined body: the forward part of the body is well rounded and the body gradually curve back from the midsection [17]. Half of the design is first created in 2-D. A reference line, 900 mm, is drawn and then a horizontal line 20 mm is created in the rear. A quarter of an ellipse is drawn from the front with radius 100 mm and a tangent line connects the top of the ellipse and the vertical line in the rear. The software function "revolve" is then used to create a volume. See Figure 4 for an illustration of the finished model. Detailed drawings are presented in Attachment 1 page 3.
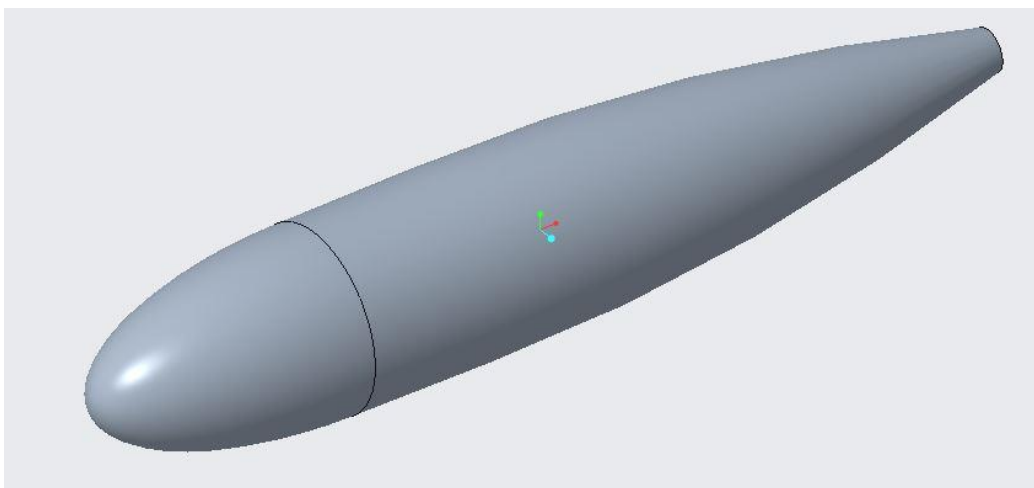

Figure 4: Reference model, teardrop shaped.

2.1.2   Irregular shape – Hvaldimir

The design goal for the experimental model is to evaluate an ovaloid hull shape for AUVs inspired by nature. In order to evaluate the difference in drag from a normal axisymmetric AUV the hull is intentionally created with a rather extreme design. This will create a baseline for further investigation.

The inspiration for the new and possibly improved design is the black tipped reef shark. This shark's frontal projected area is not circular, but oval (longer along the y-axis than the z-axis). Furthermore, it has a small elevation before the dorsal fin (the back) and slightly around the fin (stomach), a narrower body towards the back and a blunt snout. The result is a streamlined body shape, with a somewhat unusual cross-sectional area. See Figure 5 for illustration of a shark.

Figure 5: Blacktip reef shark [18].

Due to the complex shape of the shark, 22 planes are created parallel to the YZ-plane with equal spacing. In each plane a sketch is made and a guideline cross with a width to height ratio of 1.5 - width being 50% larger than the height. By further using a spline tool, an ovaloid is created by selecting each of the four endpoints of the mentioned crosses. After this the guidelines were removed and the ovaloid was split along the horizontal and vertical axis creating a sketch made up of four parts. This is repeated for all planes. By using the "blend" tool, the sketches are then linked together forming a solid body. The "revolve" tool is then used to create the ends by revolving along the z-axis with the projected edges from one side of the sketch, revolving 180 degrees.

After the initial body is created each of the sketches are adjusted to create a smooth shape with few discontinuities. Adjustments are made numerous times continuously through the CFD analysis in order to minimize the drag. The final model is presented in Figure 6. Further detailed drawings of the model are found in Attachment 1 page 1.
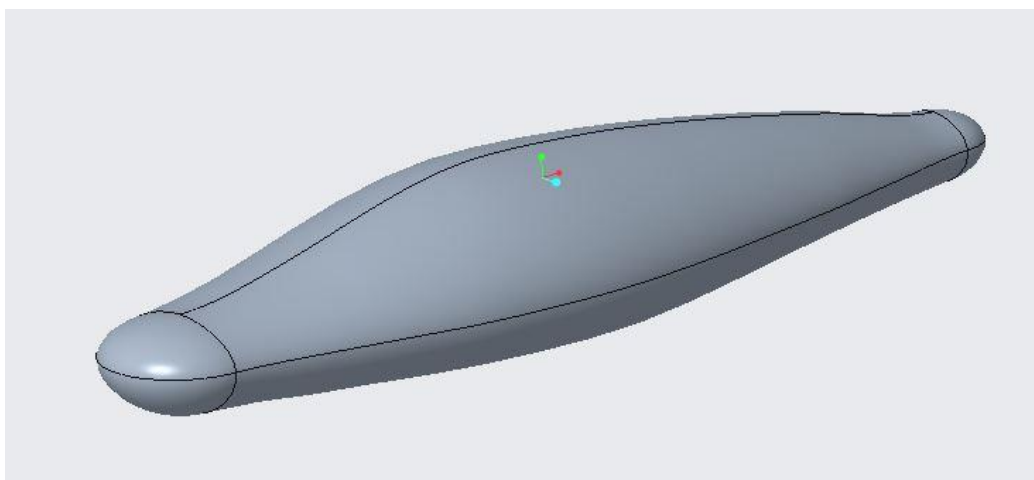

Figure 6: Hvaldimir, design inspired by the shape of a reef shark.

2.1.3 Model properties

Different model properties are presented in Table 1 for both Hvaldimir and the reference model. Comparing two different models creates a baseline for the values acquired from the CFD analysis. The reference model has a more traditional axisymmetric design and is a representation for other AUV's currently in use. One of the aims when designing the models is to ensure that the designs keep nearly the same properties, while accomplishing reduced drag force by changing the design. This similarity makes it more convenient to compare the drag coefficients mentioned later in Section 2.2.3.

Drone name	Hvaldimir	Reference model
Volume [m^3]	0.0147	0.0143
Buoyancy [kg]	14.7000	14.3425
Length [mm]	888	900
Projected area [m^2]	0.02998	0.02321

Table 1: Properties of models.

2.2 Theoretical method

Computational fluid dynamics (CFD) is the field of study devoted to solutions of fluid flow by the use of computer software. CFD makes it possible to shorten the design cycle by reducing the amount of required experimental testing [19]. Furthermore, CFD allows the user to obtain details that are difficult to obtain by experiment, such as shear stresses, pressure profiles and velocity. A theoretical explanation of fluid flow and important numbers for computational analysis are explained in this section.

2.2.1 Fluid flow

A fully immersed, streamlined body with no buoyancy and at small angles of attack will mainly experience hydrodynamic forces and moments due to pressure distribution and shear stress distribution [20]. See Figure 7Figure 7: Pressure- and shear stress distribution on a surface [16]. for an illustration of how the pressure (P) and shear stress (τ) attacks the surface of an object.

$p = p(s)$ = surface pressure distribution
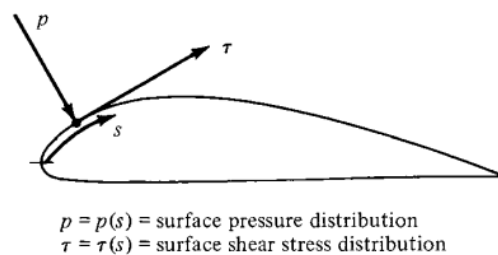$\tau = \tau(s)$ = surface shear stress distribution

Figure 7: Pressure- and shear stress distribution on a surface [16].

The sources of forces acting on a body result in pressure drag and skin friction drag. Pressure drag is caused by pressure acting normal to the surface at all points. In front of the object the fluid will be compressed and along the body the pressure will change, usually with a low-pressure region in the wake. Friction is created by the roughness on the entire wetted surface and fluid viscosity that creates an opposing force to the body's motion [21]. The fluid particles closest to the observed body will cling to the body due to viscosity, and these particles will collide with and exert shear stresses on the surrounding fluid (non-slip condition). The speed and pressure in the flow will change, from zero velocity at the side of the body, to free-stream speed, creating the formation called "boundary layer" presented by Ludwig Prandtl in the early 1900's [22]. Figure 8 presents a general form of the flow field around a streamlined body.
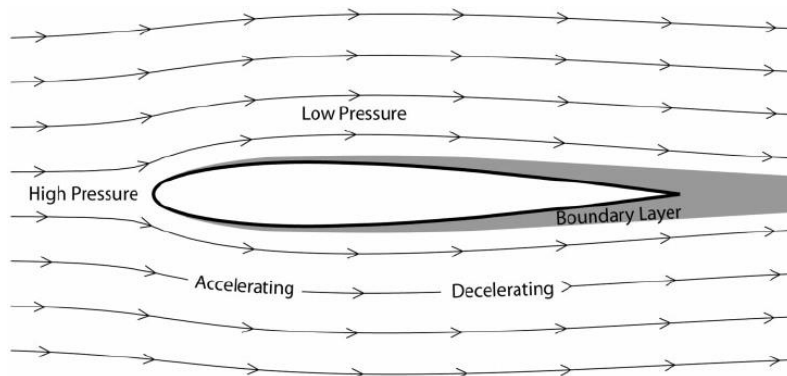

Figure 8: Flows around a streamlined body [19].

The type of flow affects the resistance the body is experiencing and is especially affected by the fluid velocity. Typically, the hull will experience orderly and smooth flow lines at the front (laminar flow) and as the fluid flows along the body the flow becomes more chaotic (turbulent flow). The turbulent flow formats a zone of swirling eddies in the body's wake and represents a decrease in the downstream

pressure on the body [17]. The details of the flow within the boundary layer and the separation point are vital when solving hydrodynamic problems. The formation of the boundary layer begins at the transition point between the laminar- and the turbulent flow and the thickness of the layer increases along the body's length. Ultimately, the boundary layer gives any design an "effective" shape that is different from the physical shape [23].

When modelling a streamlined hull, the goal is to reduce the turbulent wake, also called streamline range, as much as possible by elongating the object and reduce pressure drag as much as possible. The streamline range will generally continue a certain distance downstream from the separation point, as presented in Figure 8. However, it is important to have in mind that friction drag will increase with enlarged surface area.

In a three-dimensional flow in Cartesian coordinates, there are four coupled differential equations for four unknows (u, v, w, P') to be solved. This is a complex process and CFD is used to solve these equations. The equations of motion for a steady laminar flow of a viscous, incompressible, Newtonian fluid without free-surface effects is the conservation equation called the *continuity equation*

$$\vec{\nabla} \cdot \vec{V} = 0 \tag{1}$$

and the *Navier-Stokes equation* [19]

$$(\vec{\nabla} \cdot \vec{V})\vec{V} = -\frac{1}{\rho} \vec{\nabla} P' + \nu \nabla^2 \vec{V} \tag{2}$$

Where $\vec{V}$ is the velocity of the fluid, ρ is the density, ν is the kinematic viscosity and ∇ represents the gradient of a scalar-valued differential function. P' is the modified pressure due to the free-surface effects. The Navier-Stokes equation was derived in the early 1800's and describes how velocity, pressure, temperature and density of a moving fluid are related [24].

2.2.2 Reynolds number

In order to require a precise drag prediction using CFD it is necessary to use appropriate flow models. Today, CFD can manage laminar flows with ease, but the turbulent flows are impossible to solve without turbulence models. Turbulence models are unfortunately not universal, but standard models yield satisfactory results for most practical engineering problems [19]. Therefore, it is appropriate to find a dimensional ratio explaining the flow before starting the CFD analysis.

In 1883 Osborne Reynolds published his findings about the transition between laminar and turbulent flows, making it easier to characterize the type of flow around an object [25]. He established that the change in flow occurs when a specific combination of parameters crosses a threshold. His equation was later called Reynolds number (Re) and is a regularly utilized nondimensional parameter used in fluid mechanics:

$$Re = \frac{VL}{\frac{\mu}{\rho}} = \frac{VL}{\nu} = \frac{Inertial\ forces}{Viscous\ forces} \tag{3}$$

Here, μ is the dynamic viscosity of the fluid, ν is the kinematic viscosity and L the length. For lower Re-numbers the boundary layer is laminar and for higher numbers it is turbulent [23]. Furthermore, Reynolds number describes the ratio of inertial forces to viscous forces. The inertial forces are associated with velocity, mass or density of fluid, and explained resistance an object has towards change or motion. Typical Reynolds numbers for most fish is in the range of 1×10^5, and for large vessels or ships 1×10^9 [26].

2.2.3 The drag coefficient

In order to further understand the forces acting on the body, the calculation of drag force has been simplified by the implementation of a non-dimensional drag coefficient (C_D) [27]. The formula depends on the density of the fluid (ρ), the velocity of the object (V) and the projected area (A):

$$F_D = \frac{1}{2} C_D \rho V^2 A \tag{4}$$

For an AUV the value of C_D includes the pressure and friction drag, and is usually found by experimentation or CFD. A streamlined body has less drag than an object with a more blunt shape. In order to achieve a low drag coefficient and force, the boundary layer should remain connected to the hull as long as possible, causing a narrow wake. In Figure 9 typical drag coefficients and Re for regular 3-D objects are presented.
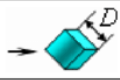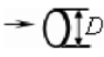
Type of body		Reference area S	Reynolds number Re	Drag coefficient C_D
Cube		$S = D^2$	$Re > 10^4$	1.05
		$S = D^2$	$Re > 10^4$	0.8
Solid hemisphere		$S = \pi D^2 / 4$	$Re > 10^4$	$\rightarrow 0.42$ $\leftarrow 1.17$
Hollow hemisphere		$S = \pi D^2 / 4$	$Re > 10^4$	$\rightarrow 0.38$ $\leftarrow 1.42$
Thin disk		$S = \pi D^2 / 4$	$Re > 10^3$	1.1
Circular disk		$S = \pi D^2 / 4$	$Re \leq 1$ $Re > 10^4$	20.4/Re 1
Sphere		$S = \pi D^2 / 4$	$Re \leq 1$ $1 < Re \leq 2\times10^5$ $Re > 2\times10^5$	24.0/Re 0.45 0.2
Streamlined body		$S = \pi D^2 / 4$	$Re > 10^5$	0.04

Figure 9: Typical drag coefficients for regular 3-D objects [25].

2.3 Numerical method

The method in this section is presented using ANSYS Fluid Flow (CFX) student version [28] and Creo Parametric. Other CFD software may yield similar, but not identical results. Thus, ANSYS Fluid Flow (CFX) is also used in order to compare data. The procedure is the same for both versions. In order to gain as physically correct results as possible, the fluid domain, meshing, boundary conditions and flow parameters should be properly generated by following the procedure below.

2.3.1   Creating the fluid domain

To create a CFD-analysis the fluid must be modelled. The principle being that a volume of fluid is created around the model being evaluated, and then the overlap between the fluid and the model is removed. The result is a void created by the model's previously occupied space where no fluid can pass through. The following paragraphs explains how to do this.

Open a new assembly in Creo Parametric. Verify that the model properties are set to millimetres to assure proper model dimensions. Import the design and make sure that the assembly coordinate system matches the model coordinate system. Use the "form new part" function to create the fluid domain. Furthermore, use the "revolve" tool in order to create a fluid domain volume.

It is vital to ensure that the fluid domain is large enough to assure proper analysis of the fluid domain. Thus, the domain should be such that the main dimensions of the fluid domain have the following dimensions: 0.7L in front, 0,6L above, and 5.5L aft [29]. Due to software limitations and complex design, the domains are created as large as possible, still ensuring a proper, regular grid later in the process.

Hvaldimir

For the shark-inspired design the fluid domain is shaped like an elongated sphere, with centre of the radiuses at the model's centreline at the end sketches in both ends. Then a horizontal line is drawn connecting the top of both circles, leaving the fluid domain with a total length of 2780 mm. Subsequently, the functions "revolve" and "boolean cut" are used to create the fluid domain. Both fluid domains are saved as a STEP file (.stp). See Figure 10 for illustration of the fluid domain for the Hvaldimir model.

Reference model

For the reference model the fluid domain is shaped like a cylinder with a circular head and radius 750 mm and total length 3425 mm. Using the function "boolean cut" the intersecting volume of the drone and fluid domain is removed. See Figure 11 for illustration of the fluid domain for reference model.

2.3.2   Separate fluid domains into subdomains

The following procedures are done using the CFD software. In order to create a CFD analysis ANSYS workbench is opened. ANSYS workbench contains several sub programs for several types of computational analysis such as Fluid Flow (CFX) which is used for CFD analysis. Once Fluid Flow (CFX) is opened the first of five subprograms starts, namely Design Modeler. In design modeler the step file is imported, and the hull design suppressed. To ensure a regular grid and reduce runtime, the fluid domain must be divided into several smaller subdomains. In order to reduce the amount of volume that is going to be meshed the model is divided into a half model, due to symmetric results on both sides of the symmetry plane. The fluid domain is then divided into subdomains using two different functions: "slice" and "extrude".

Hvaldimir

The fluid domain is sliced along the symmetry plane, and the plane perpendicular to the symmetry plane. A sketch is then created on the newly exposed symmetry plane. Exploiting this method, the drone is designed. A line is drawn at the start of the revolved part at the drone's forward and aft, which is the width of the extruded box. The extruding is done by selecting sketch and slice material all the way through. Then, select all the six bodies and group them together to one part, with the "form new part" function. This is done to ensure that the fluid will run through all subdomains. Figure 10 shows the subdomains for Hvaldimir.
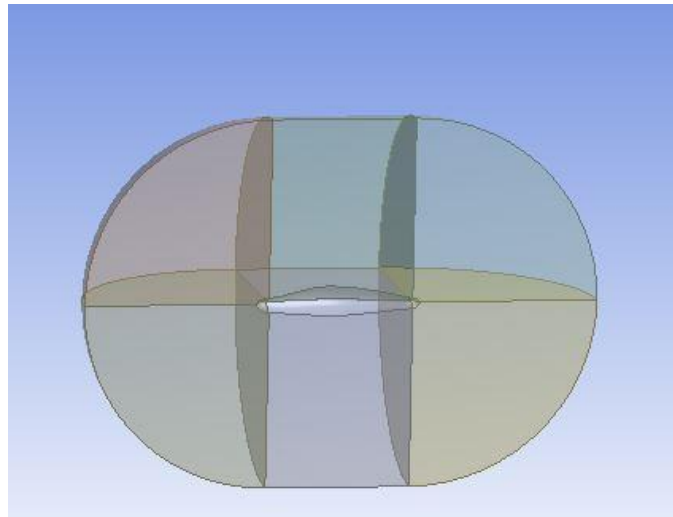
Figure 10: Subdomains for Hvaldimir.

Reference model

After importing the second fluid domain step file, the drone is suppressed. In order to divide the subdomains into four parts the "slice" tool is used in the symmetry plane and the plane perpendicular to the symmetry plane. Two of the parts are then suppressed, which leaves half a model. While remaining in the symmetry plane, a box is sketched through the fluid domain incapsulating most of the model and extruded. To ensure a proper grid in the wake of the drone, a circular sketch is created in the drones aft, and extruded through the rest of the fluid domain. Then the subdomains are selected and compiled, creating a new part. Figure 11 shows the subdomains for the reference model.
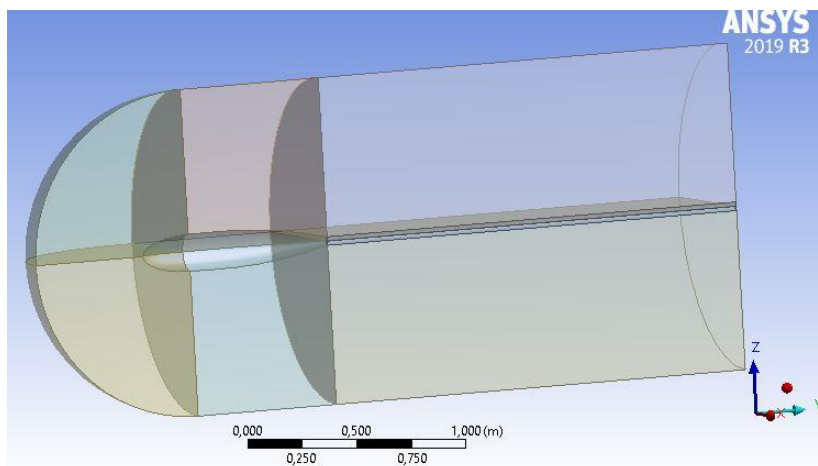

Figure 11: Subdomains for reference model.

9

2.3.3   Meshing

Once the models are divided into smaller subdomains and the hulls are suppressed, the fluid domain is opened in the meshing program. The subdomain is then further divided into several small element cells. In 3-D, these cells represent small control volumes where the equations of motion are solved. Thus, the quality of the computed solution is highly dependent on a high-quality mesh.

The higher the density of the cells are, the higher the accuracy of the results become. The grid is created with nodes and elements. The nodes are the connecting points between the elements. In ANSYS academic the number of elements is limited to 512 000, which prohibits enough cells, limiting the accuracy of the results.

Hvaldimir

To create the mesh, the following mesh boundary conditions are set to:
- Element order: Program controlled
- Element size: 30 mm
- Growth rate: default (1,2)
- Mesh defeaturing: no
- Capture curvature: yes
- Curvature min. size: 1 mm

Each of the subdomains are inserted with "sweep method": sweeping around the drone and creating a regular mesh. The sweep settings are set to a program-controlled algorithm, quadratic element order, manual source and target, element size 35 mm without bias. In order to create a regular mesh with high degree of accuracy, the element size must be as small as possible. However, element sizes smaller than 30 mm only leads to failed mesh. Many different values are evaluated in order to create the best mesh possible with the limitations enforced by the license. The details of the mesh are presented in Figure 12.

Figure 12: Mesh details for Hvaldimir.

The mesh sweeps around the y-axis. It is important to have four edges for each face in order to create a cubic mesh on every face. This results in the following meshes seen in Figure 13.
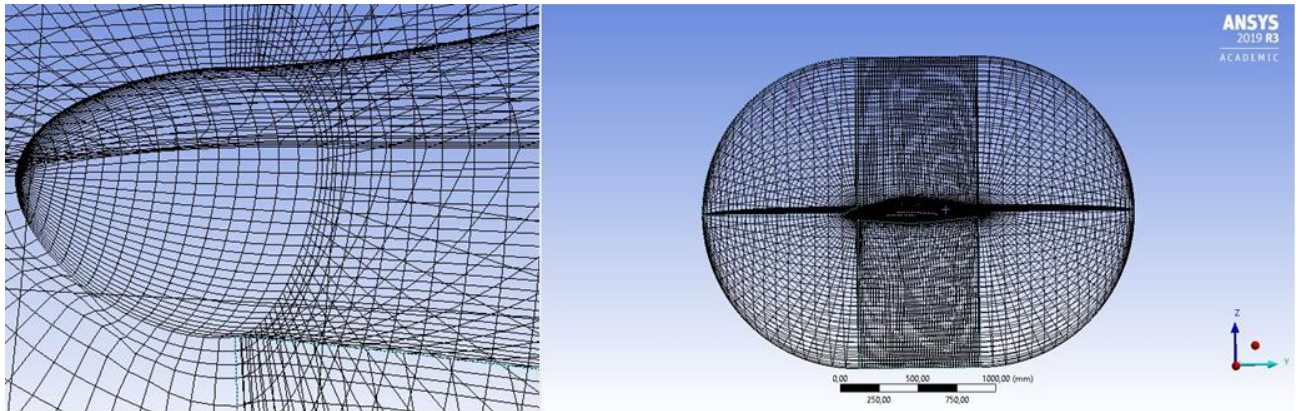

Figure 13: Detailed front mesh and total mesh for Hvaldimir.

In preparation for setup, name selections are created on the corresponding faces for inlet, opening 1, opening 2, drone and symmetry. Figure 14, Figure 15 and Figure 16 shows the name selections and the locations. The outward facing faces named 'opening and opening2' are set to opening in order to simulate endless fluid beyond the fluid domain and is a simplification in order to reduce the size of the domain. This will also reduce runtime. The symmetry name selection is created in order to run a halve model analysis. Inlet name selection is created in order to define where the fluid velocity comes from. The Drone name selection is created in order to create a smooth wall on these faces in the solver.
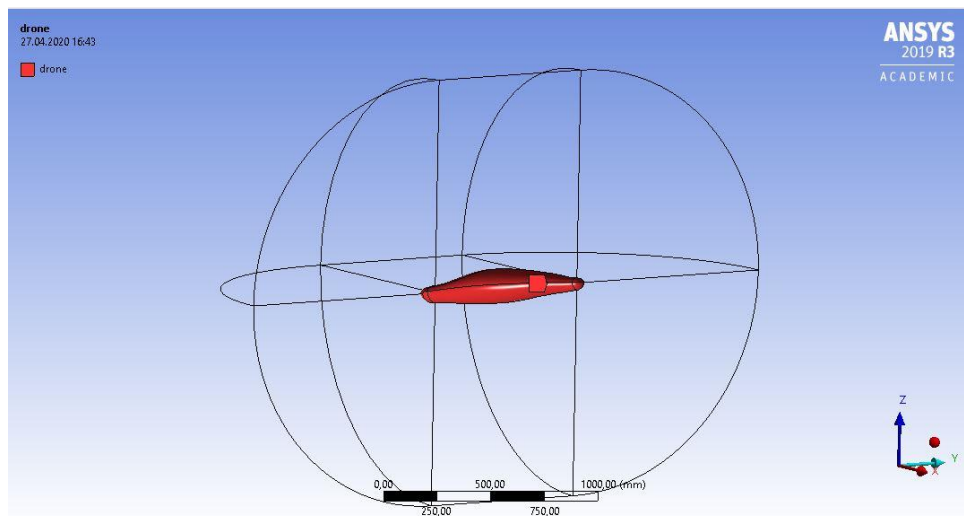

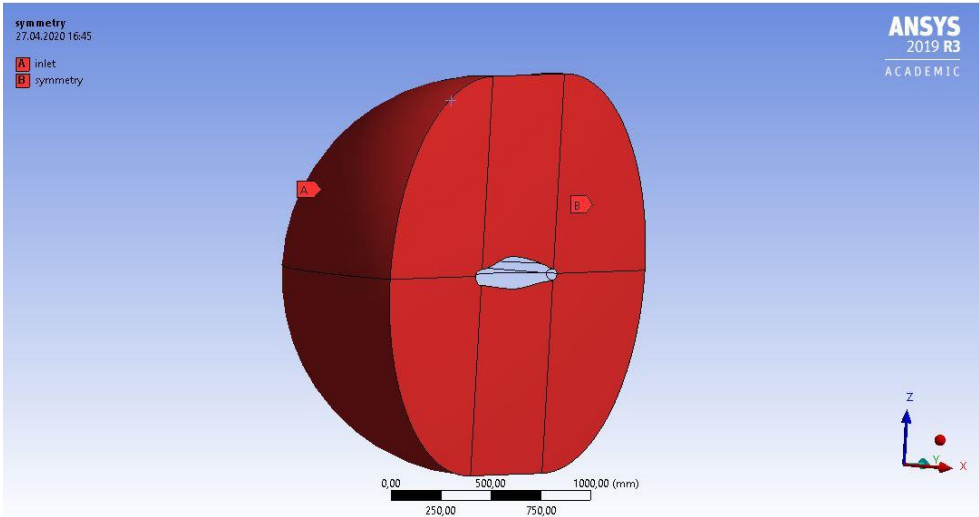Figure 14: Name selection for drone related faces.

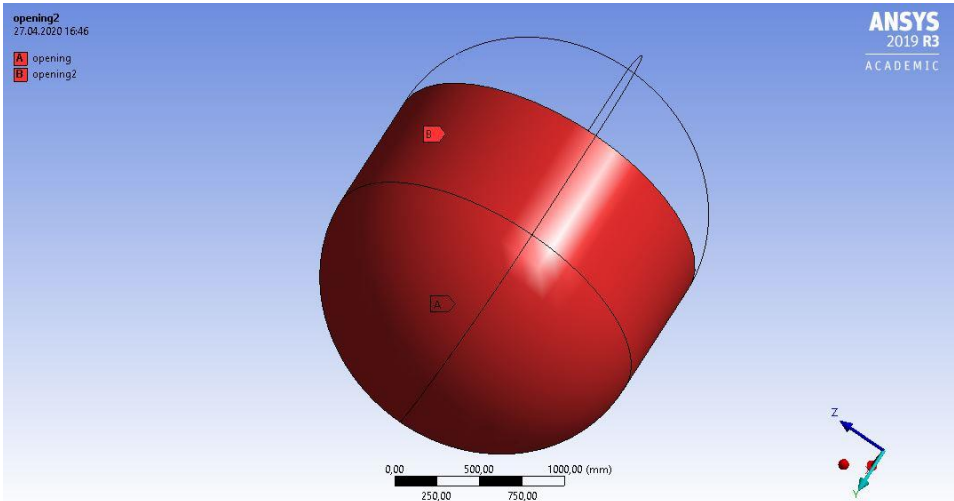Figure 15: Name selection for faces of inlet [A] and symmetry plane.

Figure 16: Name selection for opening [A] and opening 2 [B].

Reference model

The details of the mesh for the reference model are presented in Figure 17. The subsequent procedure for creation of mesh the reference model is the same as presented above for Hvaldimir.Figure 12

Figure 17: Mesh details reference model.

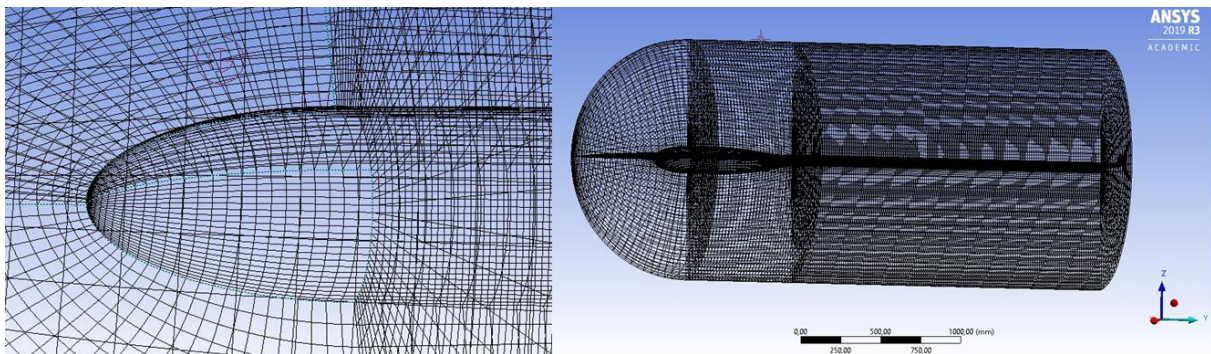This results in the following meshes for the reference model – see Figure 18 .

Figure 18: Detailed front mesh and total mesh for reference model.

In preparation for setup, name selections are created on the corresponding faces. See Figure 19 and Figure 20 for the name selection locations.
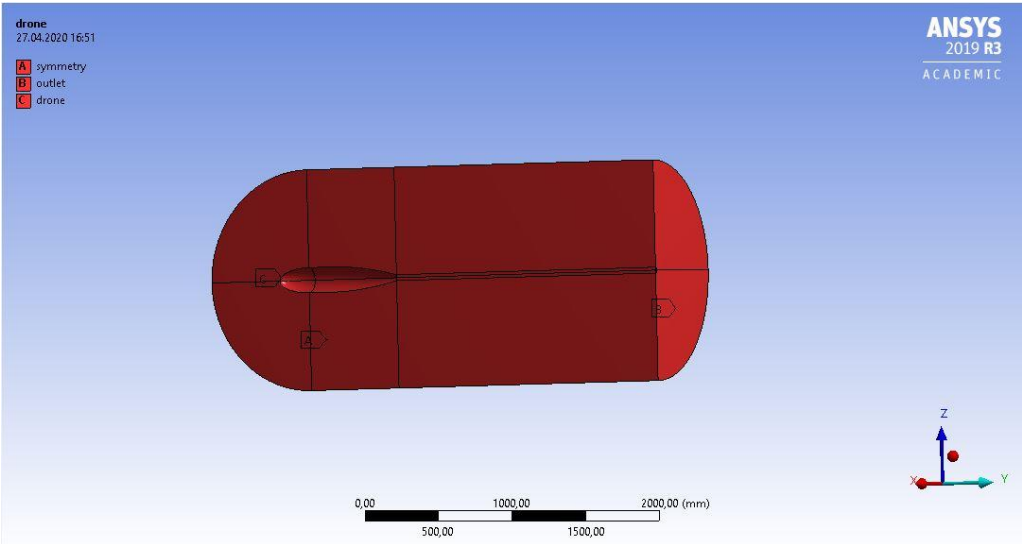
Figure 19: Name selection for symmetry plane [A], outlet [B] and drone [C].
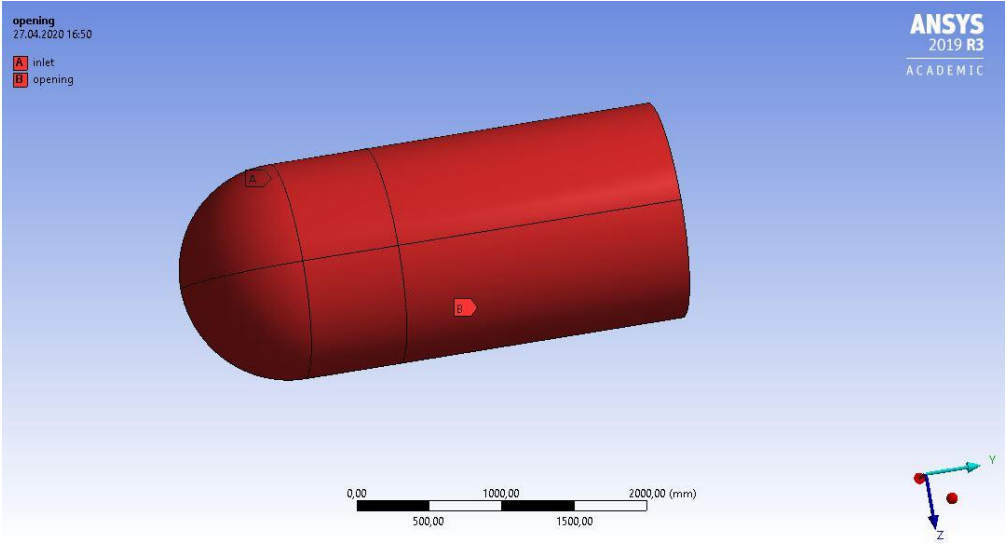

Figure 20: Name selection for inlet [A] and opening [B].

Mesh comparison

The main differences of the meshes are displayed in Table 2. As most other parameters are equal, the number of elements, nodes and element sizes are the biggest differences and are therefore compiled in the table. All though the license for student version of the software limits the number of nodes and elements to 512 000 this does not seem to be absolute. Shown by the large number of nodes in the mesh for the reference model. The low number of elements in the mesh for Hvaldimir is due to the 30 mm limitation of minimum element size. The reference model's element size is set to 20 mm, as a further decrease would lead to too many elements in the mesh.

	Hvaldimir	Reference model
Number of elements	145314	347380
Number of nodes	596678	1421850
Element size	30 mm	20 mm

Table 2: Mesh comparison, Hvaldimir and reference model.

2.3.4 Setup

In the setup program CFX-Pre, the boundary conditions and turbulence model are added. The boundary conditions in the default domain are adjusted in the following way for simulation of both Hvaldimir and the reference model Figure 21.
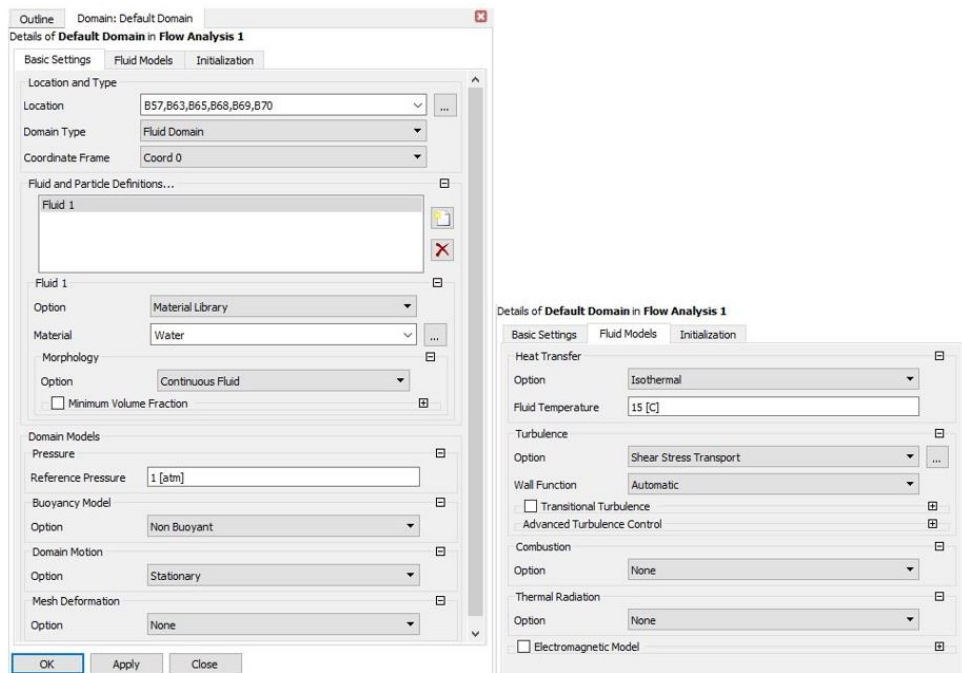
Figure 21: Boundary conditions for models.

The fluid is set to water from the material library, Reference pressure 1 [atm], non-buoyant buoyancy model. The domain motion option is set to stationary as the simulation is not dependent on changes in time. Heat transfer is set to isothermal at 15° [C]. The turbulence model is set to shear stress transport as by advice from CFD consultant Dr. Mariusz Domgalansa, as it is more accurate for low Reynolds number simulations.

Due to the spherical shape of the inlet on the fluid domain, Cartesian velocity components are chosen. The velocity of the fluid is flowing towards the front of the drones, which results in a velocity along the y-axis, the V cartesian velocity vector. The velocity varies from 0.5 m/s to 5 m/s with 0.5 m/s increments.

Hvaldimir

The following Table 3 presents the setup for Hvaldimir.

Location	Basic setting	Boundary details
Inlet	Boundary type: Inlet	Flow regiment: subsonic
		Mass and momentum: Cartesian velocity component, U= 0 m/s, V=x m/s (varying from 0.5 to 5 m/s), W=0 m/s
		Turbulence: medium (intensity=5%)
Opening 2	Boundary type: Opening	Flow regiment: subsonic
		Mass and momentum: entertainment
		Relative pressure: 1 [atm]
		Turbulence: zero gradient
Opening	Boundary type: Opening	Flow regiment: subsonic
		Mass and momentum: entertainment
		Relative pressure: 1 [atm]
		Turbulence: zero gradient
Drone	Boundary type: Wall	Mass and Momentum: no slip wall
		Wall roughness: smooth wall
Symmetry	Boundary type: Symmetry	

Table 3: Setup for Hvaldimir.

Figure 22 illustrates the fluid domain achieved by following the presented setup.
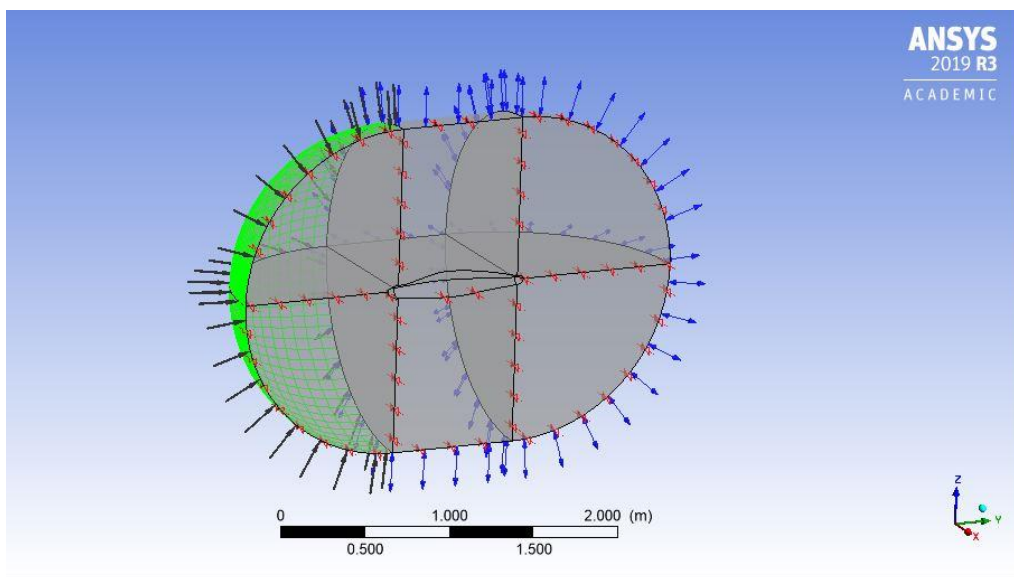

Figure 22: Fluid domain with setup vectors for Hvaldimir.

Reference model

Table 4 presents the setup for the reference model, and Figure 23 shows the fluid domain.

| Location	Basic setting	Boundary details
Inlet	Boundary type: Inlet	Flow regiment: subsonic
		Mass and momentum: Cartesian velocity component, U= 0 m/s, V=x m/s (varying from 0.5 to 5 m/s), W=0 m/s
		Turbulence: medium (intensity=5%)
Drone	Boundary type: Wall	Flow regiment: subsonic
		Mass and momentum: no slip wall
		Wall roughness: smooth wall
Opening	Boundary type: Opening	Flow regiment: subsonic
		Mass and momentum: entertainment
		Relative pressure: 1 [atm]
		Turbulence: zero gradient
Outlet	Boundary type: Opening	Flow regiment: subsonic
		Mass and momentum: entertainment
		Relative pressure: 1 [atm]
		Turbulence: zero gradient
Symmetry	Boundary type: Symmetry	

Table 4: Setup reference model.
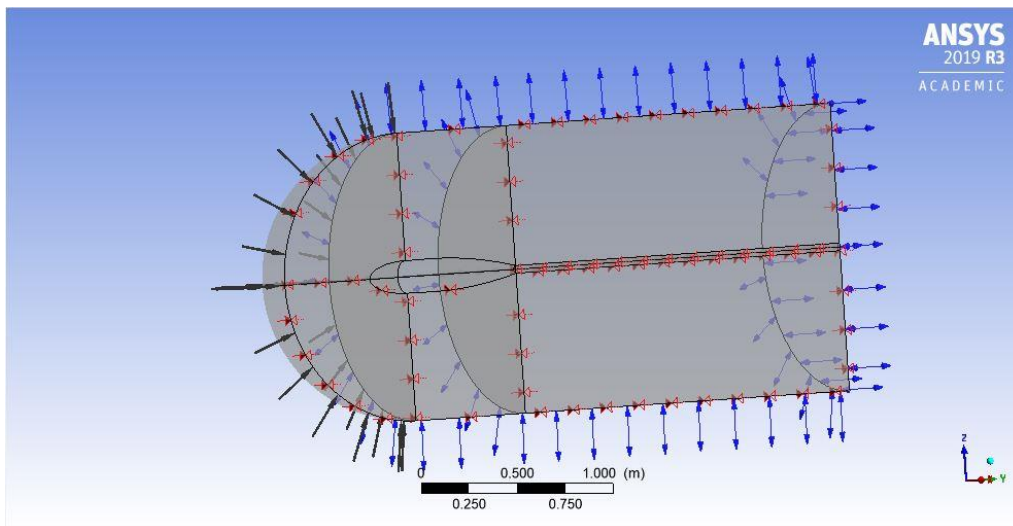
Figure 23: Fluid domain with setup vectors for the reference model.

In preparation of the solution, the "solver controller" is adjusted with convergence control: minimum 1 iteration, and maximum 300 iterations. Convergence criteria residual type RMS, and residual target: 1.E-4. These are the default settings for the program.

2.3.5   Solver

The following solution is found with CFX Solver Manager. The settings are set to double precision, and the solver is started. To ensure that the setup is created properly, the graphs created by the solver is monitored closely. The solver ran smoothly and reached the residual goal in less than 100 iterations.

2.3.6   Results

When the solver is complete, the CFX-post program is opened, and the drag force is calculated using the function calculator. Selecting the forces along the y-axis acting on the drone name selection provides the resulting drag forces. This result is compiled in a table for further numerical analysis. To visualize the flow characteristic around the model, contours are created on the symmetry plane with velocity as a variable. A pressure contour on the drone name selection is also created to visualize the pressure distribution on the drone body.

This process is repeated for each of the ten velocities evaluated in the assignment for both Hvaldimir and the reference model. This allows for creation of graphs comparing the results from the CFD analysis.

2.3.7   Creating a reference model without streamlined design

In order to compare the effect of a streamlined body a cylindrical model is created. This is done to evaluate a model with high induced turbulence behind the model, in comparison to the two streamlined drones Hvaldimir and the reference model. The streamlined drones should have a more laminar flow over the body, which reduces the turbulence behind the model as well as the drag. This is due to less pressure reduction behind the model.

The cylinder is created with the "revolve tool" by sketching a sphere with radius 100 mm, followed by a 800 mm horizontal line parallel to the x-axis. A vertical line with length 100 mm is then drawn from the x-axis to the horizontal line. To close the sketch, a horizontal line is drawn from the top of the extremal point of the semicircle to the vertical line along the x-axis. Finally, a centreline is drawn along the x-axis. The 2D sketch is then revolved along the centreline 360 degrees, creating the model shown in Figure 24.
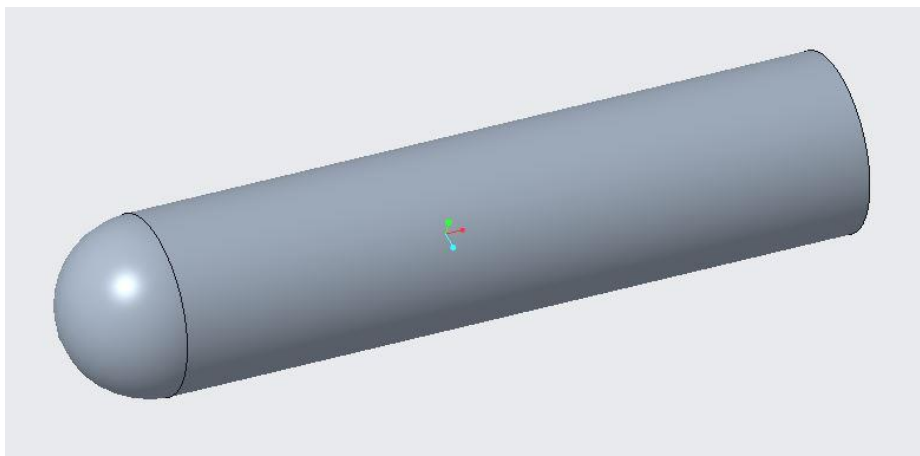

Figure 24: Modelled cylinder.

2.4 Preparation for experimental method

Software analysis of hydrodynamic parameters have limitations and often rely on empirical relations found though physical tests. Due to this, physical model testing remains significant. Therefore, two drones are created to confirm the CFD tests. The model creation and plan for experimental testing are presented below.

2.4.1   Creation of models

When creating physical drone models, finding an effective production process is important to allow for thorough towing tank testing in the allotted time window. For maximum flexibility during construction, a combination of foam plates and industrial glue is used for easy hull shaping and optimal compatibility with the CNC machine. *Divinycell* foam plates are used as they are very light, easy to shape with hand tools, and react well with the chosen glue. Figure 25 shows how the plates are measured before cutting.
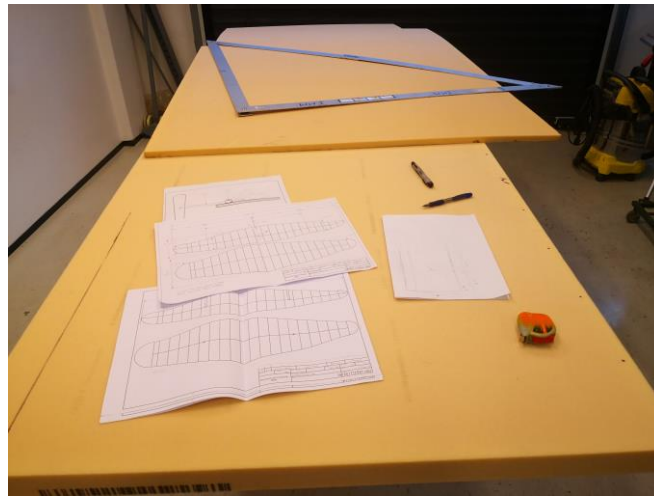

Figure 25: Measuring and preparing the Divinycell plates for cutting.

The plates are cut in pairs of four, with a length of approx. 100cm and width of 19cm. These plates are then glued together by using *BT Multibond Rapid* (Art.nr. 36-4832, Biltema), as shown in Figure 26. The result is a foam cuboid ready for processing by the CNC machine, where four similar pieces is then shaped into the hull of the reference model and Hvaldimir.

Figure 26: Divinycell plates after gluing, preparing for further treatment.

To create attachment points for the MarinLab towing rig, a plasma cut iron plate is fitted in the middle of the cross section. The milled plate as well as the ballast rods are then welded together, encapsulated by the two foam halves, creating the desired hull shape. The iron plate in the middle creates two sturdy connection points to the MarinLab rig with neutral buoyancy provided by the ballast rods for optimal towing tank stability, as shown in Figure 27 and Figure 28.
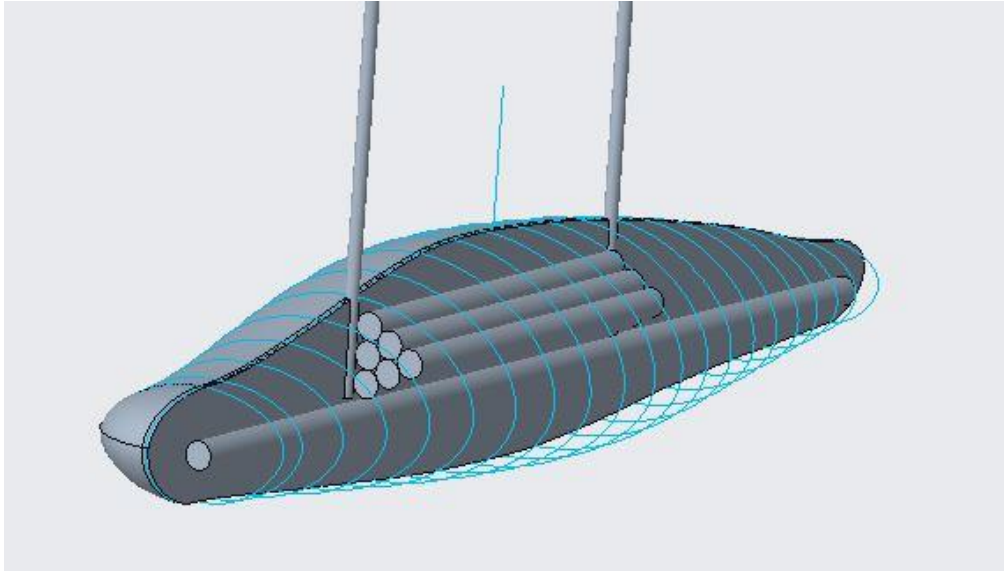

Figure 27: Ballast rods Hvaldimir.
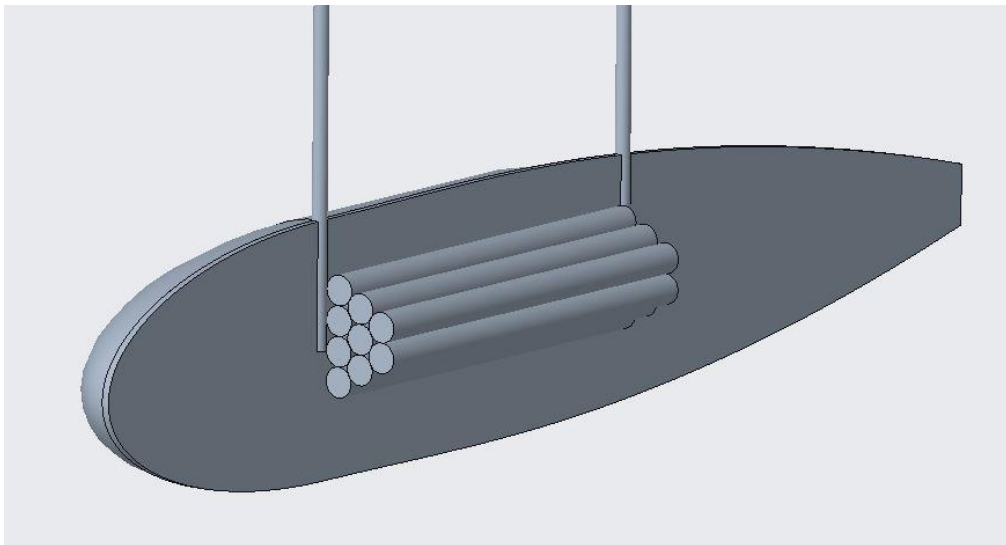
Figure 28: Ballast rods reference model.

The CNC process leaves a rough surface on the foam hull, unfit for testing in a wet environment – see Figure 29. To prepare for the waterproof coat of paint, the surface is covered in a resin-primer mix to smooth out any roughness left behind by the manufacturing process. The mix is administered by hand, as it is easy to distribute over the surface of the drone. After administering the solution, rough sandpaper is used to remove any excess resin mix, readying the drone for further treatment.

Figure 29: Drone hull halves with space for ballast rods, after epoxy and sanding.

As reducing the drag is the main goal of this thesis, the outer finish is very important. Therefore, to create a smooth surface, extensive sanding of the exterior is done with 400 grit size sandpaper. This provides a better surface for the primer and spray paint, which in the end will make the surface silky smooth after several coatings of paint. Both drones should have approximately the same finish, as this will give the most accurate results when trying to identify the most effective hull shape.

The experiment is designed to be executed in a towing tank that allows the model to be dragged through the water at various speeds. In order to submerge the model completely and keep it at a steady depth a trolley attachment is designed. This will hang under the wagon at four attachment points and allow detection of forces – see Attachment 1 page 8. The trolley attachment allows small deflections in axial direction which can be detected with a load sensor, while simultaneously stopping movement upwards and sideward. The attachment enables pitch adjustment which can be used to verify that the model is level compared to the water surface. Any angle of attack will contribute to increased drag due to an increase in projected area. Figure 30 illustrates the test set up with a model and the full drawing is presented in Attachment 1 page 5.
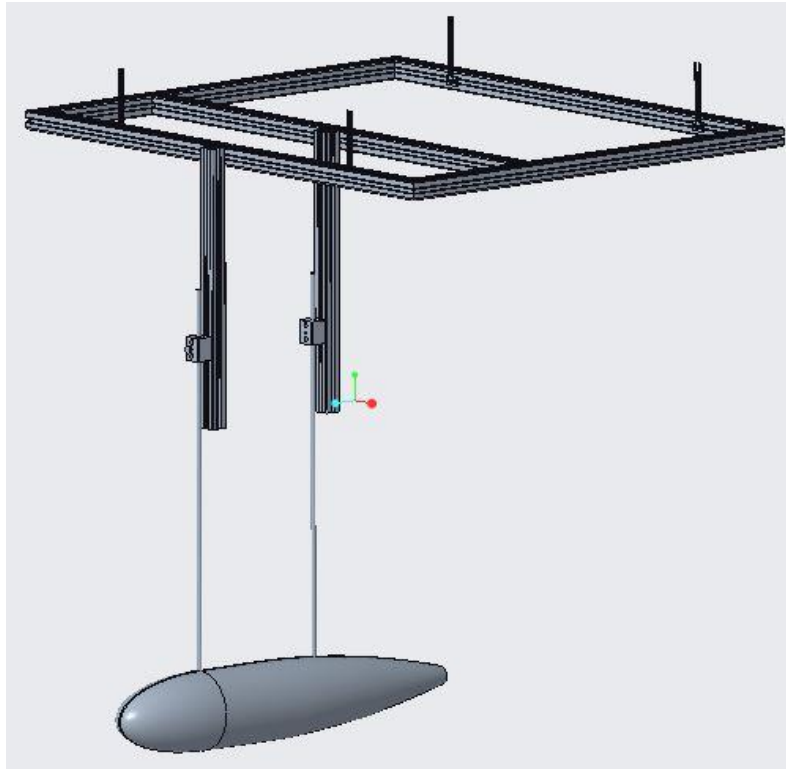
Figure 30: Test set up with model.

The trolley attachment is created with square aluminium pipes which creates a stable platform with little deformation with the expected loads applied from the models. There are two square aluminium pipes, described in Attachment 1 page 6, attached vertically to the main square frame. These are adjusted such that the lower end is 40 mm above the water surface. On these pipes two aluminium blocks with holes are attached, one on each pipe. The metal rods welded to the metal mid-plate inside the drones (Attachment 1 page 2 and 4) are attached with a 6 mm bolt to the blocks. As shown in Figure 31, this ensures a secure connection between the frame and the model.
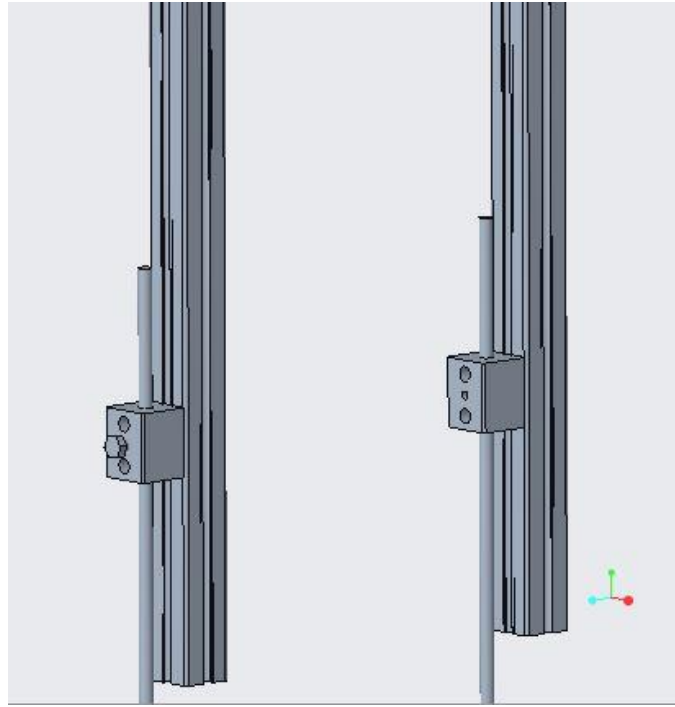
Figure 31: Square aluminium pipe and block.

The square aluminium blocks used to secure the metal rods is designed to accommodate adjustment in height, both on the aluminium pipe as well as on the metal rod attached on the drone. The metal block is created by cutting a square aluminium block into a rectangle with length 50mm. A hole is created top down with a diameter of 11 mm where the model rods will be inserted. On the front of the blocks a total of 5 holes are drilled, two all the way through, and the remaining three only partly through the piece. These are drilled to accommodate screws that will attach it to the aluminium pipe, in order to secure the metal rod as shown in Figure 32. The edges on the piece are sanded down to create a chamfer. For drawings see Attachment 1 page 7.
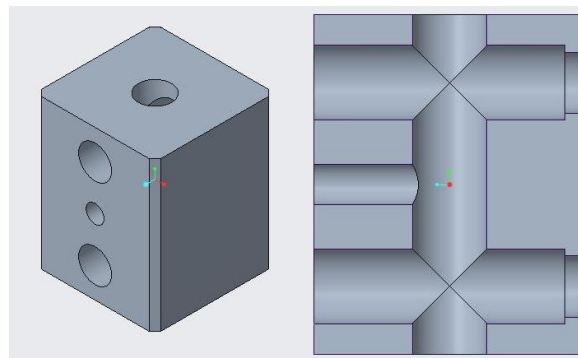

Figure 32: Aluminium block connecting the drone to the rig.

2.4.2   Model testing

To achieve the wanted results, both drones are put through the exact same procedure, at the same speed increments. The goal is to perform a total of ten tests which will give ten drag values corresponding to their speeds. These values will prove if the proposed hull shape is more effective than the reference model.

Test procedure

- *The model is attached to the MarinLab rig through its four anchoring points*
- *The attachment for load cells is mounted and load cells are attached*
- *The load cells are activated and connected to the MarinLab monitoring system*
- *The operator confirms there are no waves or movement in the water to reduce the chance of inaccurate readings*
- *The model accelerates to the chosen speed using the pulley system*
- *The speed is kept constant for at least 10 seconds or more*
- *It is recommended to repeat some tests (2-3) to examine accuracy and find standard deviations*
- *The mean value for the period of constant velocity is calculated and used in the further analysis*

This process is repeated for each drone, with one test per speed increment. The chosen speeds ranges from 0.5 m/s up to 5 m/s, with an increase of 0.5 m/s per increment. This provides twenty data sets in total, ten for each drone, which will give a clear representation of the drag for each drone design.

The results provided by the physical test is forfeited as the towing tank tests could not be completed, and the numerical testing described in section 2.3.4 will replace the towing tank results.

2.5 Sources of error

Due to surface roughness from construction and the following surface treatment, resistance caused by friction on physical models will be significantly higher than smooth simulated ones. These factors are more prominent when testing in a towing tank, as the surface finish must be smooth to minimize the factors affecting drag. However, when testing in a CFD environment, a lot of the inaccuracies from the experimental method are removed as the surface friction is a set value in the software. On the other hand, this assumes that the CFD software is configured correctly, which cannot be sufficiently proved until confirmed by the towing tank results. This means that both methods have pros and cons regarding the accuracy of test results, and both methods should complement each other for best results.

2.5.1 Numerical method

- Student version limitations on mesh resolution
    - Version used in the tests has a strict limit on nodes and elements, reducing accuracy in the simulations
    - Results will give a rough estimate, but for accurate results either a towing tank test or a simulation in the full version should be completed
- Small differences in vetted surface and reference area for Hvaldimir, reference model and cylinder

2.5.2 Experimental method

- Drag induced by the iron rods connecting the drone to the load cells will create extra turbulence which are not included in the CFD analysis.
    - CFD analysis of the rods results in an expected force nearly three times as large as the force on the drone models (Attachment 3, figure "Drag force on supporting rods")
    - Running towing tank tests with only the rods can give a good baseline for tests with drone models
    - Subtracting the baseline force calculated for the rods from the total force found in towing tank tests with drone model gives the force on the drone
- Water movement and waves from earlier tests in the towing tank can affect results
    - Every test completed will create some waves in the tank, which can affect later test results if not given time to rest
    - The operators should wait until the water calms between each test to minimize this effect
    - Tests done at higher speeds require more waiting, as more waves are generated
- Less time to measure results at higher speeds due to length of towing tank
    - At higher speeds, the drone uses a significant amount of time to accelerate to the chosen velocity. This provides less time to measure drag, which means less accuracy on the test results
    - At lower speeds, the drone can reach the required speed quickly, resulting in a longer window to collect measurements
    - Drag tests at lower speeds have more data points to generate results from, and will therefore be more accurate
    - At low speeds, the signal noise can be large relative to the measured drag, leading to inaccuracies measuring the low drag values.
- Difference between the speed registered at the pulley system and the speed measured from the MarinLab measuring systems have a deviation of approximately 0.001-0.005 m/s

3. Results

Section 3 presents results from the hydrodynamic calculations done by CFD for both Hvaldimir and the reference model. In the following section figures of fluid domain properties, drag force and drag coefficients at different velocities are presented. Furthermore, a comparison between the results from the student version and full version software are introduced.

3.1 Reynold numbers

Mostly dependent on drone velocity and geometry, the Reynolds numbers show how the fluid flow will behave when in proximity of the drone as well as in the following wake. In Figure 33, the two models' Reynolds numbers are compared to see which model has the most significant effect on the water flow. A low Re-value implies lower drag and less flow disturbance. It is to be noted that the values for Hvaldimir and the reference model are relatively similar, as the length and velocity are almost identical for both drones.
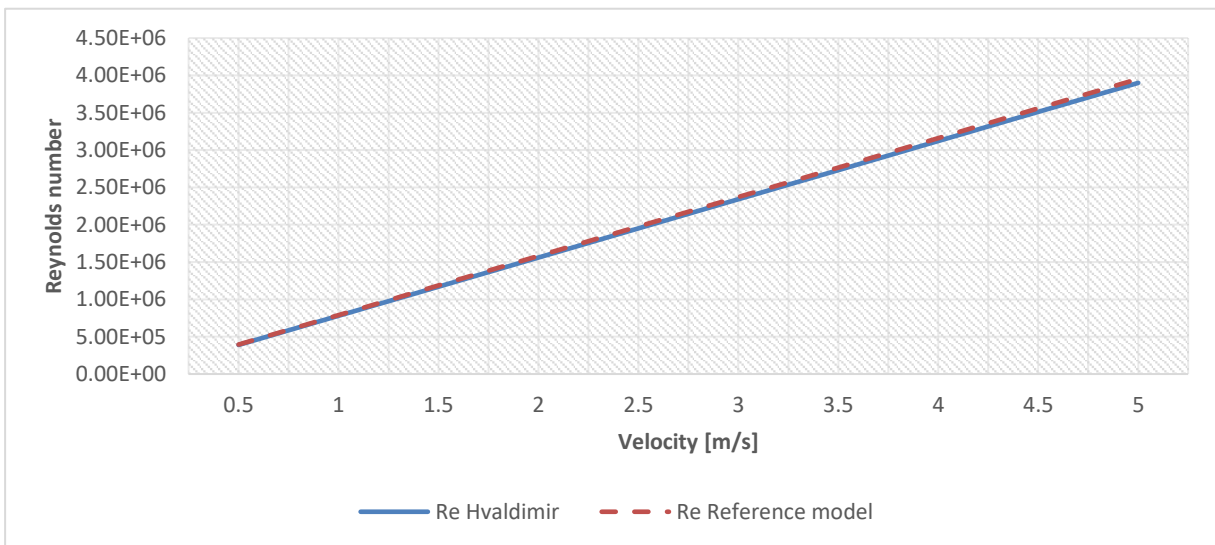

Figure 33: Comparison, Reynold numbers.

3.2 Renders of properties in fluid domain and on drone body

After examining the fluid flow using CFD the physical properties such as velocity, pressure and turbulence can be presented. In the following sections renders of fluid flow of all models are presented and commented on. The scale to the left represents the magnitude of the properties and the scale on the bottom represents length. All renders display physical phenomena at velocity 5 m/s. The pressure, velocity and turbulence are linear, and a decrease in velocity would linearly decrease the value of velocity, pressure and turbulence. The shape and size stay constant for every velocity, but the value of the scale on the left side of the renders varies. Fluid flow properties such as pressure and velocity at other velocities are displayed in Attachment 2.

3.2.1 Hvaldimir

The velocity in the fluid surrounding Hvaldimir is displayed in Figure 34. The inverse proportionality of velocity and pressure is clearly shown on the maximal thickness of the drone body. The area of high velocity corresponds with the area of low pressure on the drone body. This may indicate an area of separation which could prove disadvantageous for the drone. Areas of lower velocity is also visible in front, behind and in an area near the drone's front. The area in front of the drone corresponds with a high-pressure area on the nose, where the fluid initially contacts the drone body. The wake of the drone is produced by a turbulent low-pressure area caused by the volume of the drone body. This is visible in Figure 36.
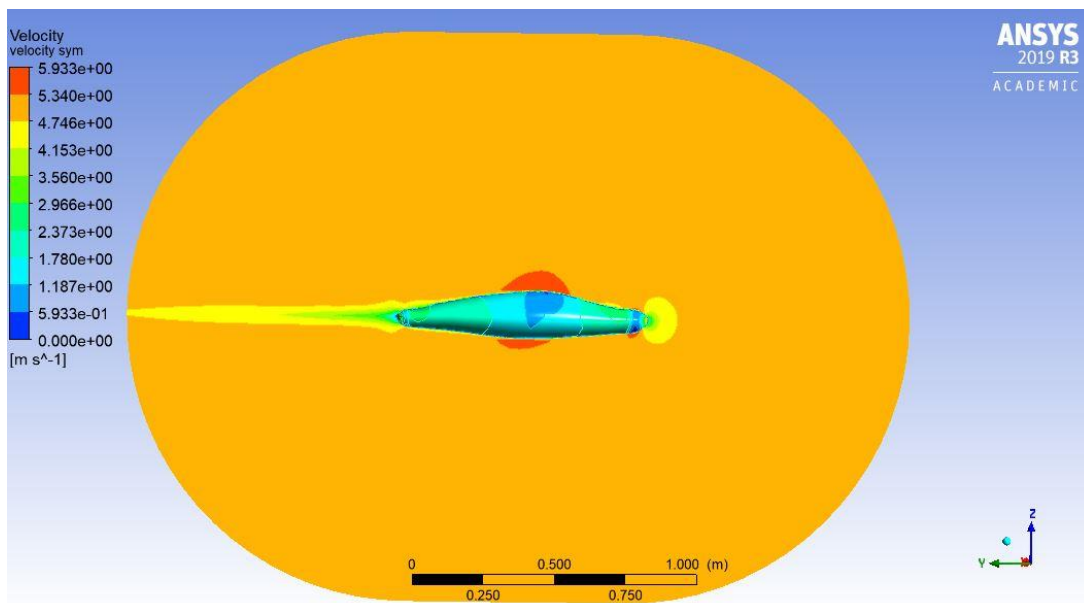

Figure 34: Velocity distribution around Hvaldimir.

The low velocity area on the drone's top side is visible in Figure 35, and corresponds with an increase in pressure due to a relative sudden incline change along the top.
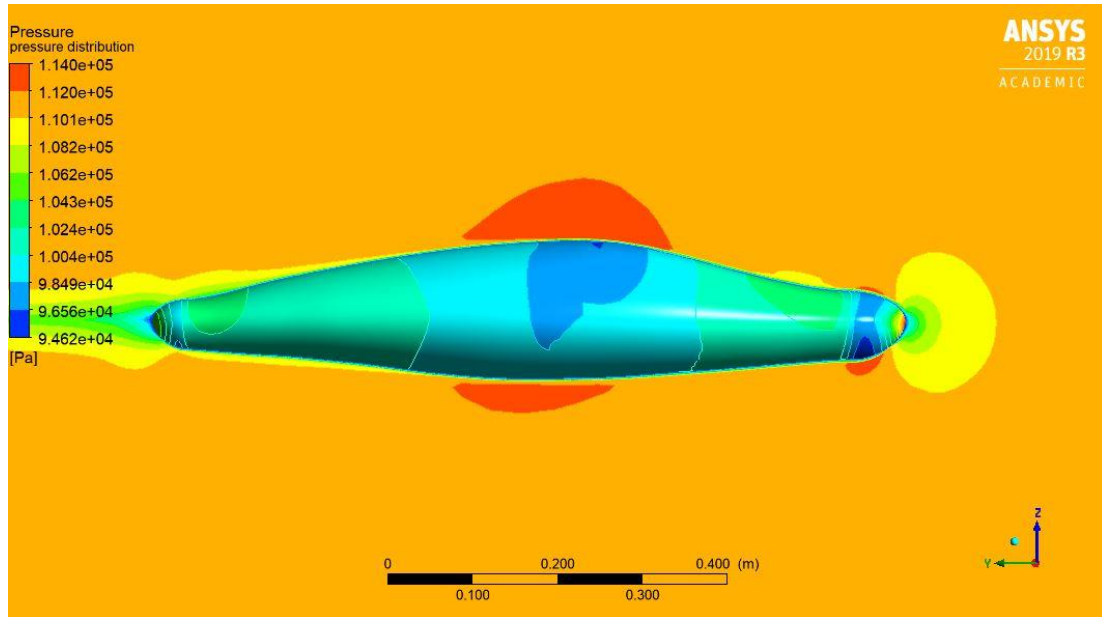
Figure 35: Pressure distribution on Hvaldimir.

In Figure 36 the pressure distribution on the drone and in the surrounding fluid is displayed. There is a visible correlation between the pressure distribution in the fluid and on the drone. The increase of pressure on the drone's nose induces an increase of pressure in the fluid further ahead. This again leads to a reduction in velocity in this area. There is also a correlation between the areas of reduced velocity on the top side, both in front and behind maximum diameter.
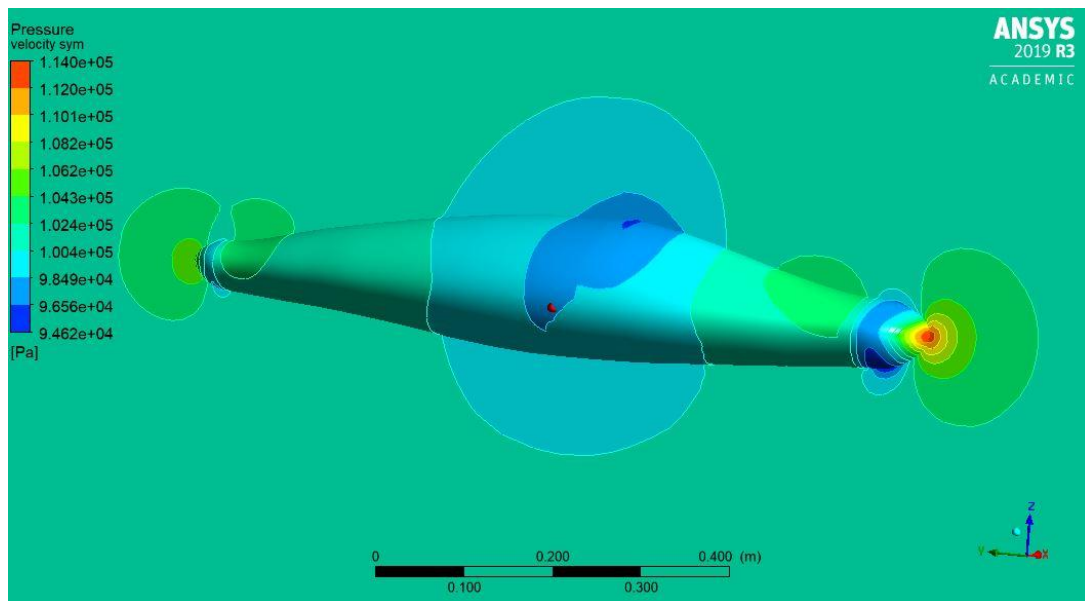

Figure 36: Pressure distribution in water, Hvaldimir.

3.2.2 Reference model

Figure 37 presents areas of low fluid velocity displayed using the colours yellow and green. High velocity in front, along the hull, and in the wake corresponds with theory. In the areas of low velocity, there is high pressure, as presented in Figure 38. There is no distinct pressure and velocity change at the middle section of the reference model as seen on Hvaldimir.
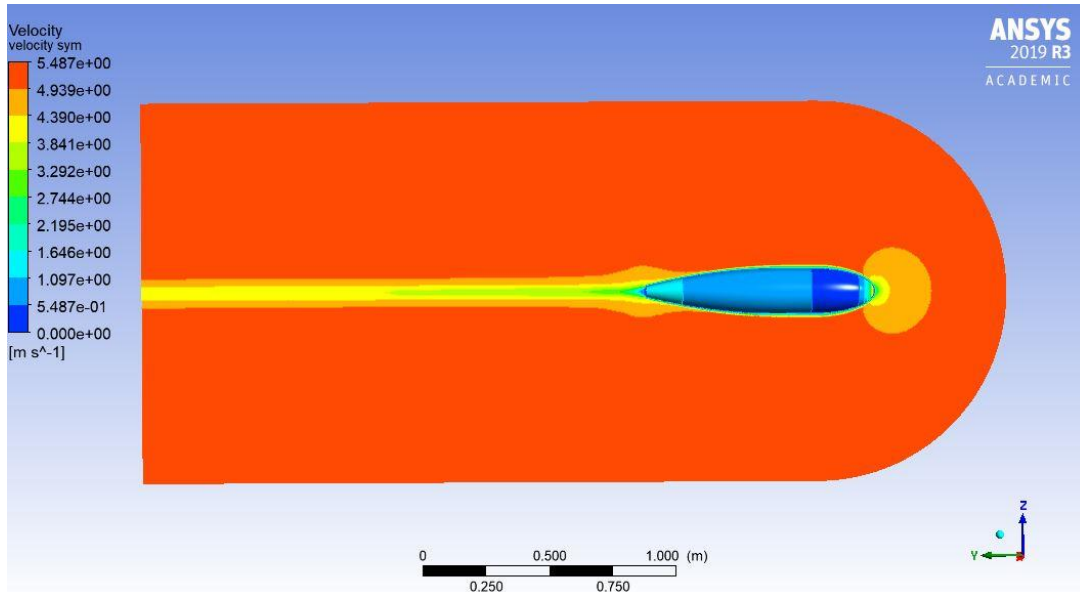

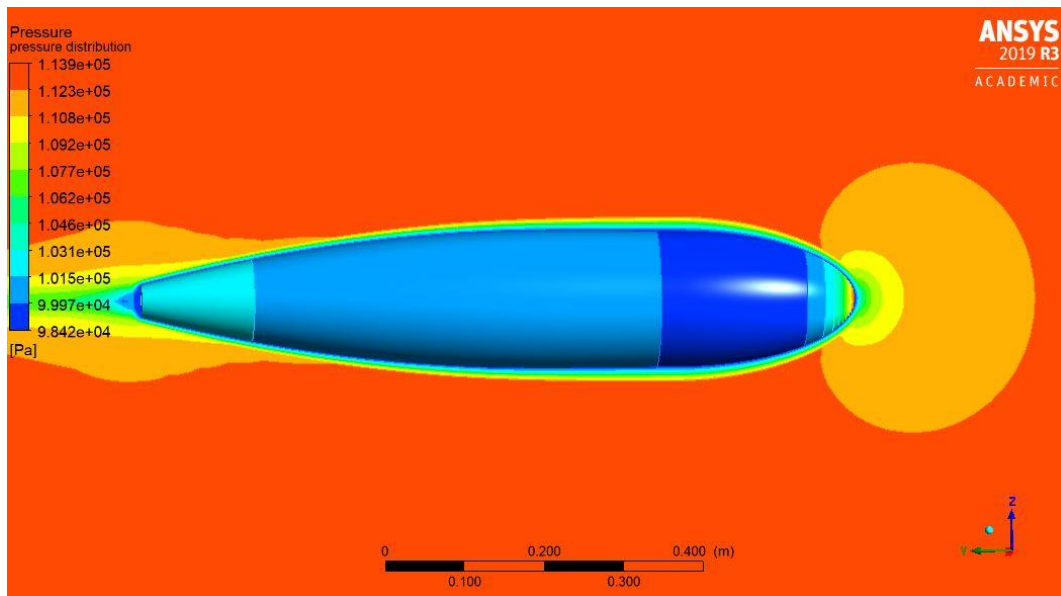Figure 37: Velocity distribution reference model.

Figure 38: Pressure distribution on reference model.

Figure 39 presents the pressure distribution in the fluid due to the model's movement. High pressure, presented in red, where both the fluid and the hull in front contributes to decreasing velocity. There is an area behind the front with low pressure, which corresponds with a slight increase of fluid velocity as it is forced to pass around the shape of the drone.
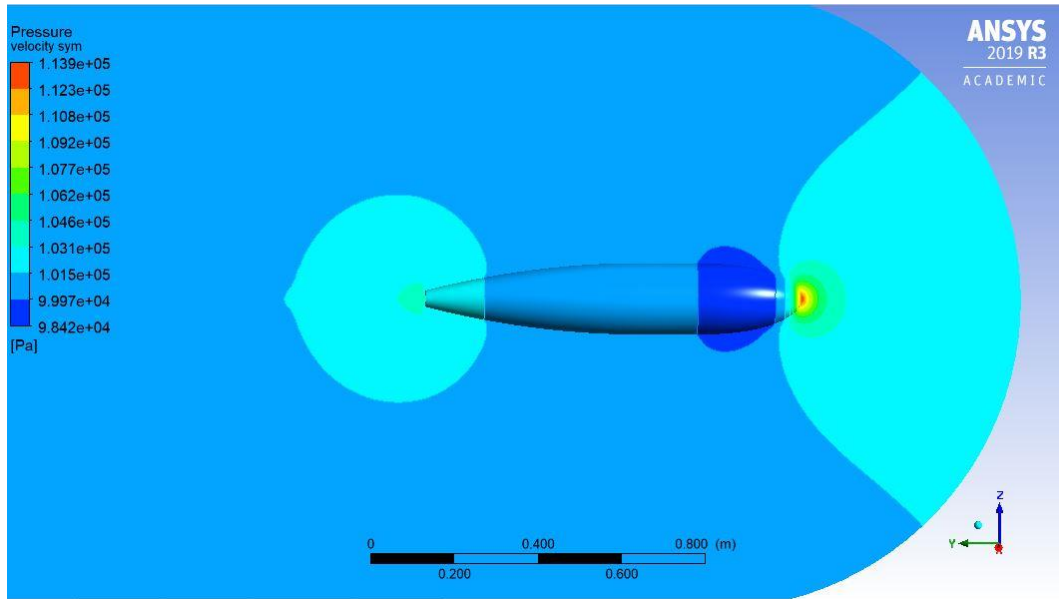
29

Figure 39: Pressure distribution in water, reference model.

3.2.3   Wake comparisons

Comparing the turbulence kinetic energy displayed on the symmetry plane for each of the three models gives a visible inclination of the degree of turbulence created by the model when traveling through the fluid. Optimal design would reduce turbulence behind the model, which minimizes pressure drop and further mitigates drag induced by this low-pressure area.

Hvaldimir

For Hvaldimir there is a slight increase in turbulence behind the maximum diameter shown in Figure 40. This might indicate separation from the drone body. Furthermore, there is a small area with increased turbulence close to the drone's tail, indicative of the pressure reduction in this area. The wake is less than one body length.
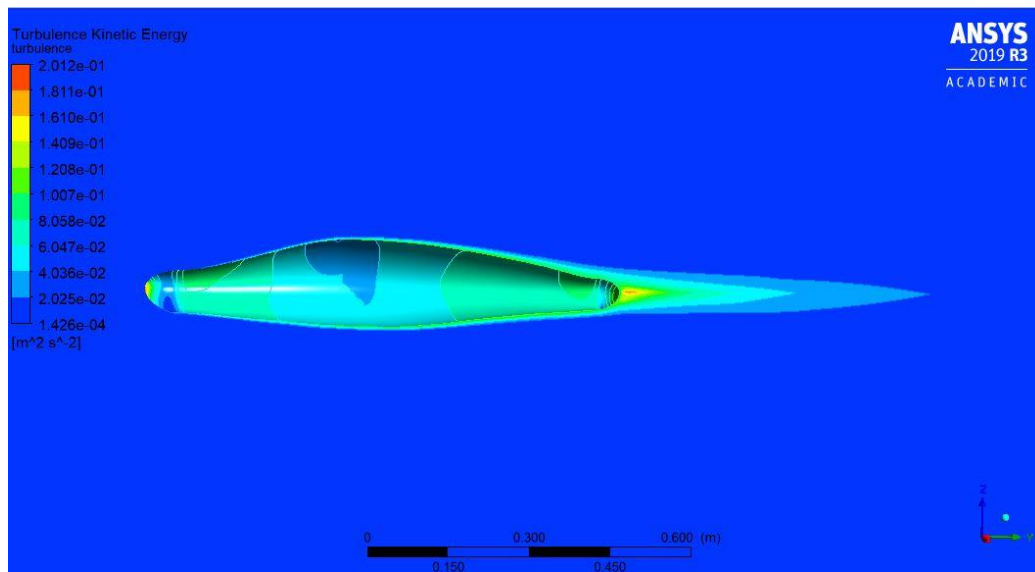

Figure 40: Hvaldimir, wake.

Reference model

In Figure 41 the turbulence in the fluid surrounding the reference model is displayed. It seems to be a slender area of turbulence along the body length after maximum diameter, this may indicate separation. The turbulence behind the drone is much less prominent compared to Hvaldimir in Figure 40. The turbulent area is shorter than the body length, apart from some areas of turbulence which might be a faulty result by the program.
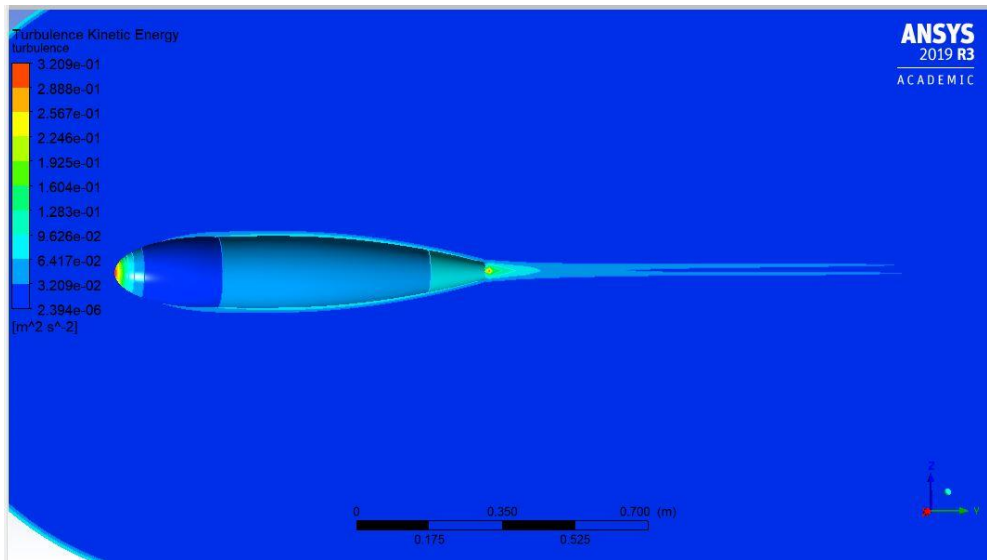

Figure 41: Reference model, wake.

Cylinder

In Figure 42 the turbulence behind the cylinder is displayed. There is a substantial amount of turbulence, and the turbulence wake is longer than the body length. This is induced by the abrupt sharp edge on the cylinders aft.
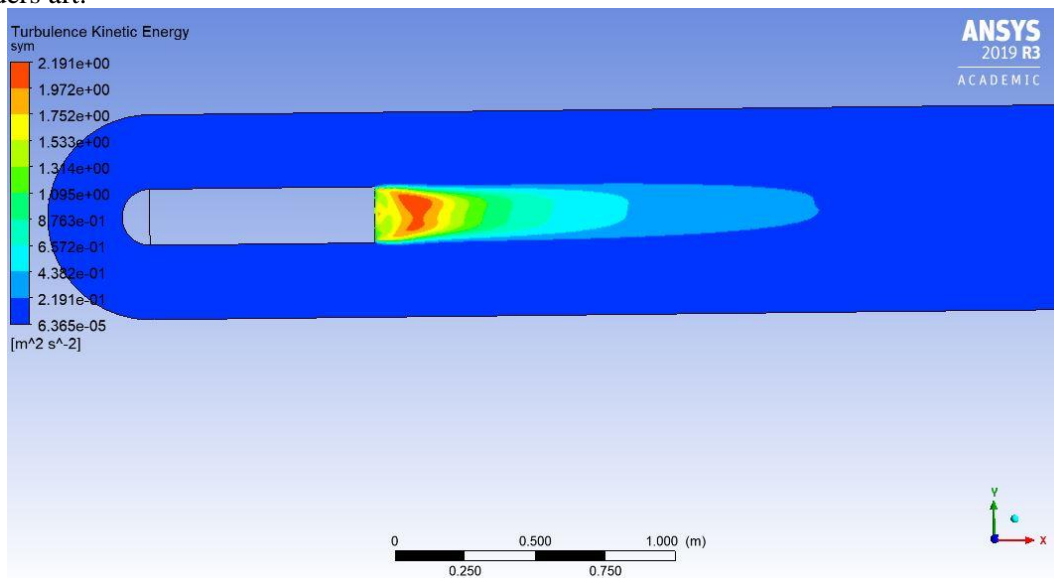

Figure 42: Cylinder, wake.

3.3 Drag force and drag coefficients

Figure 43 presents the correlation between drag force and velocity – higher model speed ultimately causes higher resistance from the fluid. Hvaldimir and the reference model have approximately the same values. The cylinder has distinctly higher drag force than the other models.

Figure 43: Drag force and velocity.
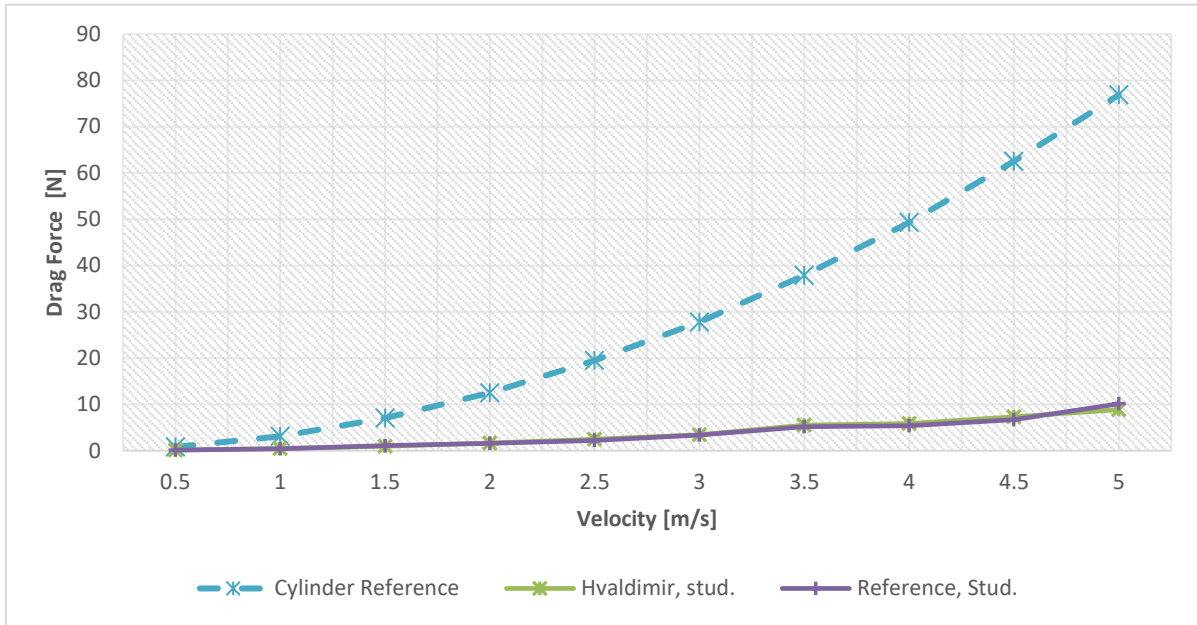
Figure 44 presents a focused comparison of Hvaldimir and the reference model. As mentioned earlier, the relationship between drag force and velocity of the hulls are relatively similar. However, the reference model has slightly lower drag force at most velocities. After 3.5 m/s irregularities for both models are visible.
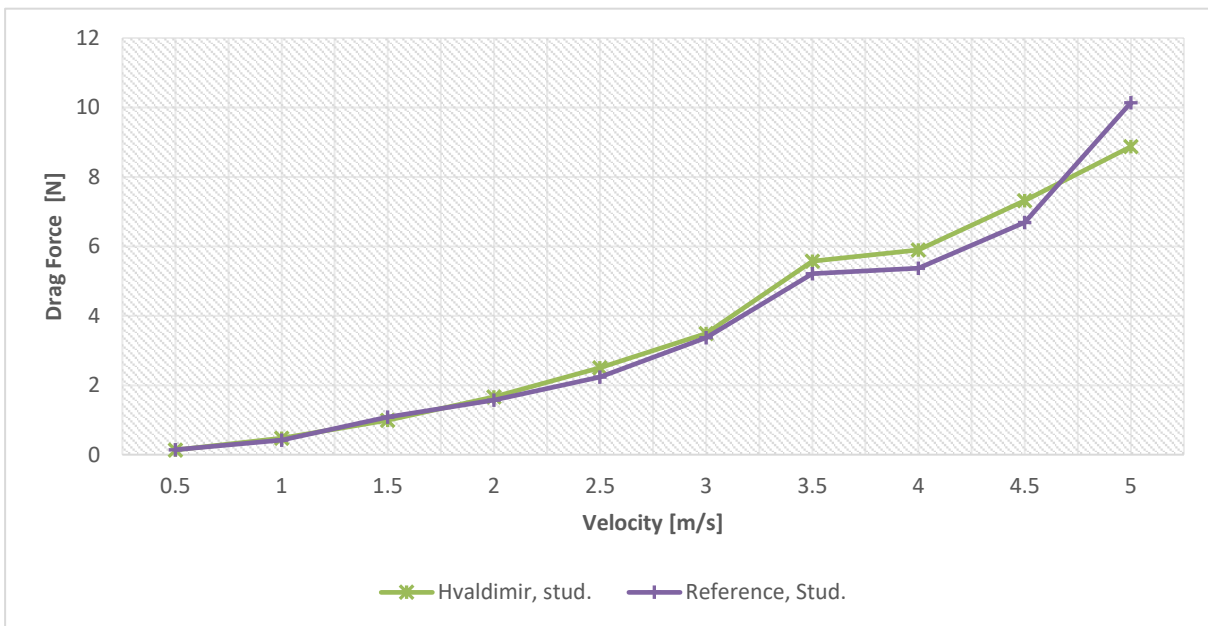
Figure 44: Drag force and velocity, Hvaldimir and reference model.

Based on Formula (4) the drag coefficient is calculated at different velocities. In Figure 45 the relationship between drag coefficient and velocity is presented. The drag coefficient decreases with higher velocities. The drag coefficient of Hvaldimir is less than the for the reference model at all velocities. Some deviations are also visible, especially for the reference model.
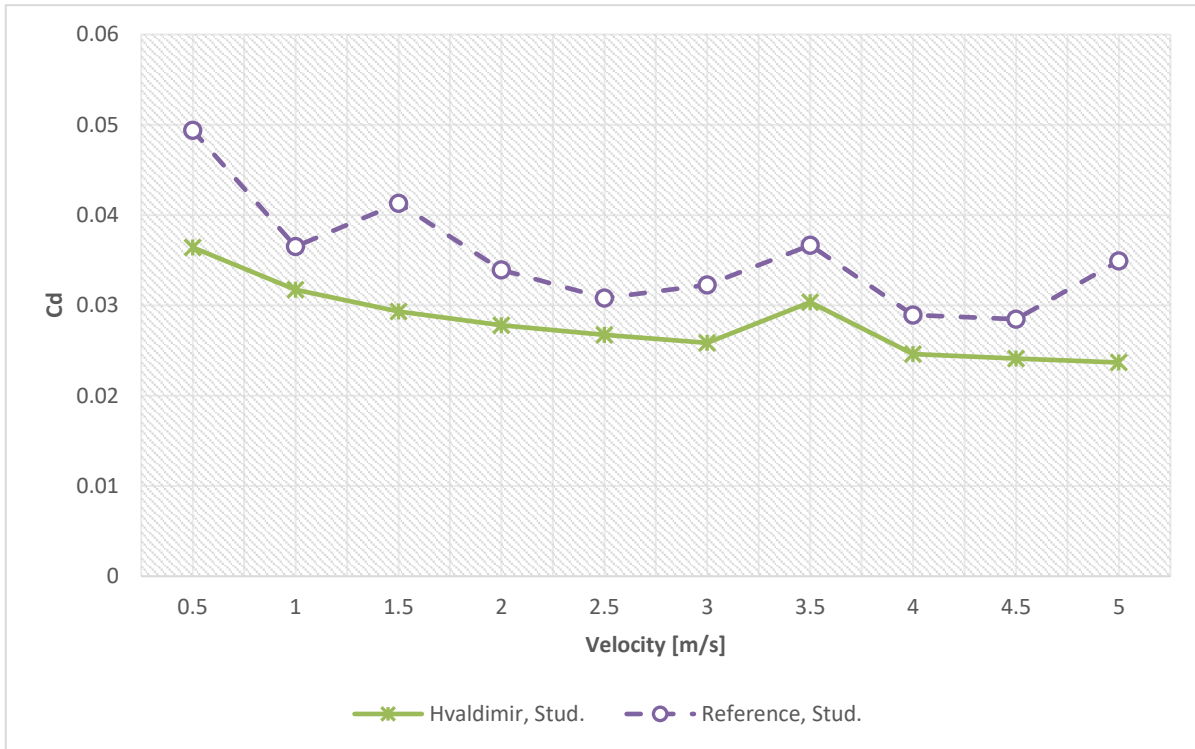
Figure 45: Drag coefficient and velocity, Hvaldimir and reference model.

As the Reynolds number increases, the velocity increases and ultimately also the drag force. This is presented in Figure 46. It is proportional with Figure 44.
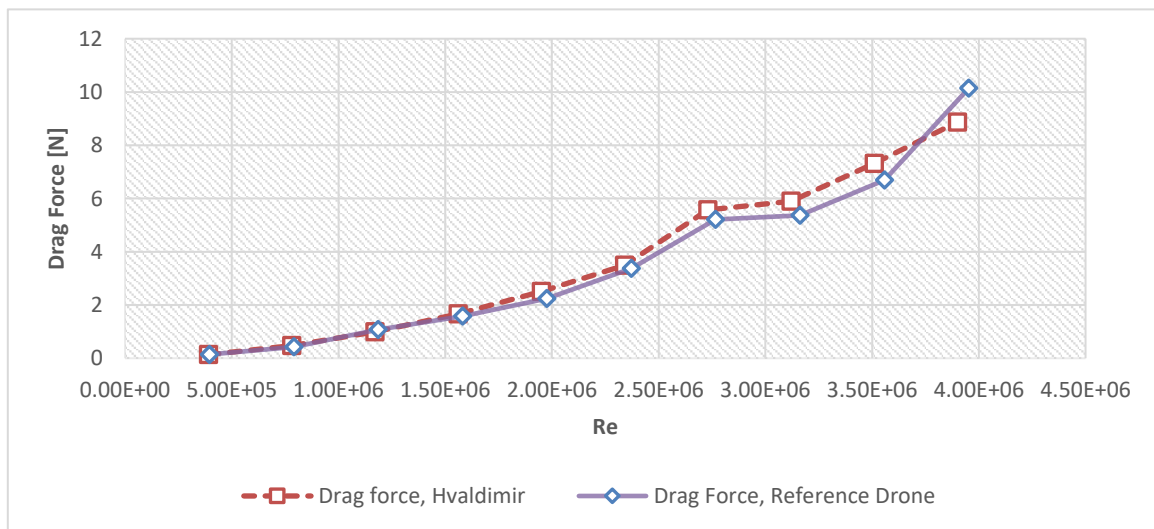
Figure 46: Drag force and Reynolds number, Hvaldimir and reference model.

3.4 Comparison, ANSYS CFX full- and student version

Figure 47 presents a comparison between the full version and student version. The full version of the software calculates higher drag forces without any deviations. Furthermore, Hvaldimir has higher drag forces than the reference model. This corresponds with the results from the student version below 3.5 m/s.
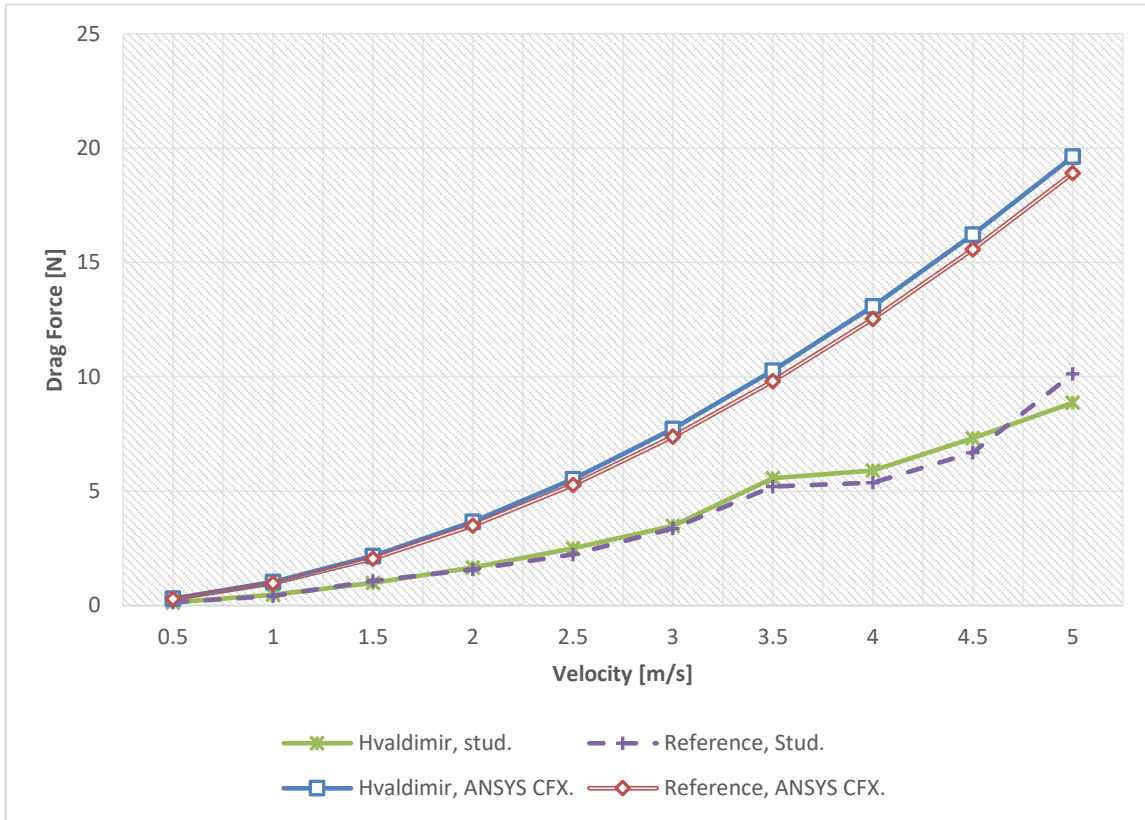
Figure 47: Drag Force, ANSYS CFX full version vs ANSYS CFX student version.

In Figure 48 the drag coefficients calculated in both software versions are compared. The drag values are overall lower in the student version, while the full version software shows a somewhat higher coefficient on both drones. However, both drones share similar trendlines.

Figure 48: Drag coefficient, ANSYS CFX vs. Student version.

4. Discussion

Due to the nature of the chosen task, developing an improved hull is a problem which can be approached from a multitude of directions. This means that finding the perfect design can only come through experimentation with hull shapes in ways that usually would not come to mind. In order to asses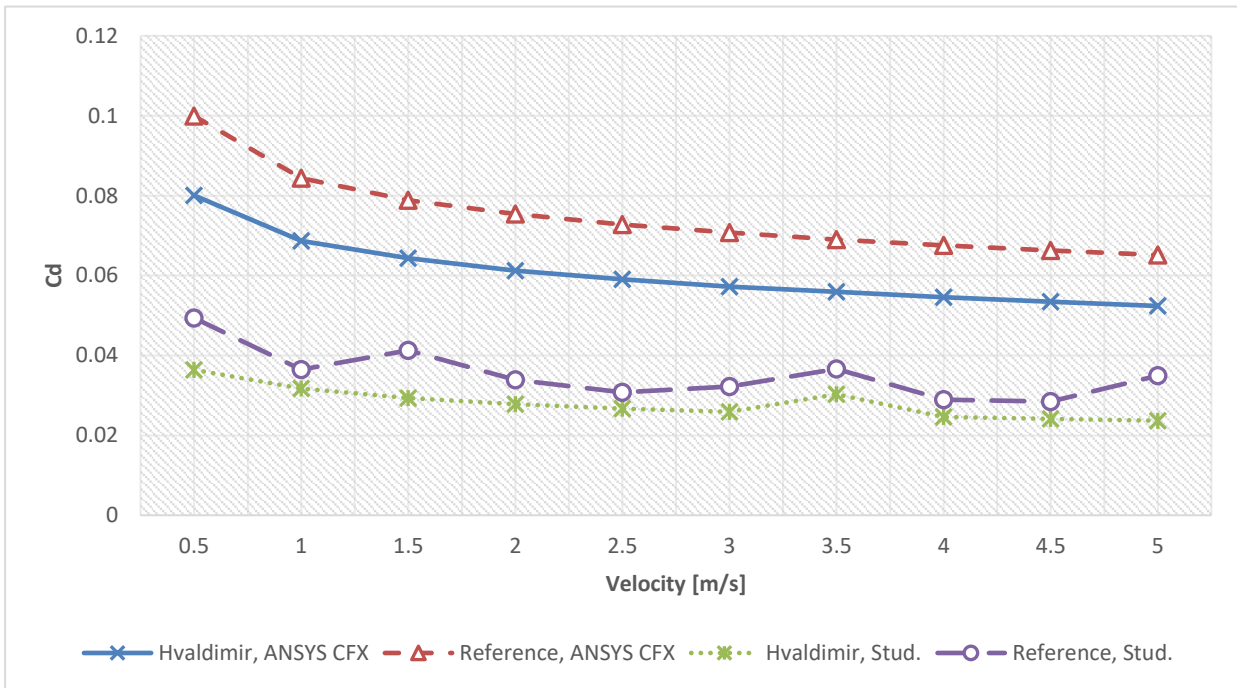s a well-proven shape from nature, a Hugin-like model was created to compare our design with a realistic model. The drones designed in the report both have a relatively similar width-to-length ratio of 1/5, based on the original Hugin's dimensions of 1-meter width and length of 5 metres.

For further research on a drone's behavior in a fluid, adding external equipment can give valuable insight about drag generated by objects mounted on the hull. This could be accomplished with relative ease in a towing tank, compared to running a new CFD analysis for each iteration. This would make it convenient to explore different external equipment configurations in the towing tank, where something like a universal mount on the drone would allow hot swapping between different equipment in a range of shapes and sizes. As these antennas are a vital component in today's AUVs, there is a significant interest in evaluating the drag increase caused by these components. This is simplest to do in towing tanks.

When testing submerged vehicles in a setup such as proposed in Figure 30 the drag force induced by the vertical metal rods should be reduced. This can be done by creating a more aerodynamic shape that can be placed around the rods. An oval shape created with a 3D-printer might be a suitable solution.

After thorough testing of both hull variants, a version 2.0 of Hvaldimir was proposed but not included in the current test results. Figure 49 is a model of the newer version of the drone. This version had an even 'flatter' projected area to further experiment with the biological shape concept, as the flatter shape had lower drag in some test results. This model also eliminated the turbulent areas seen in Figure 34, especially surrounding the drone's 'nose'. This is the drone suggested for further analysis as it looks to be the obvious evolution of Hvaldimir 1.0.
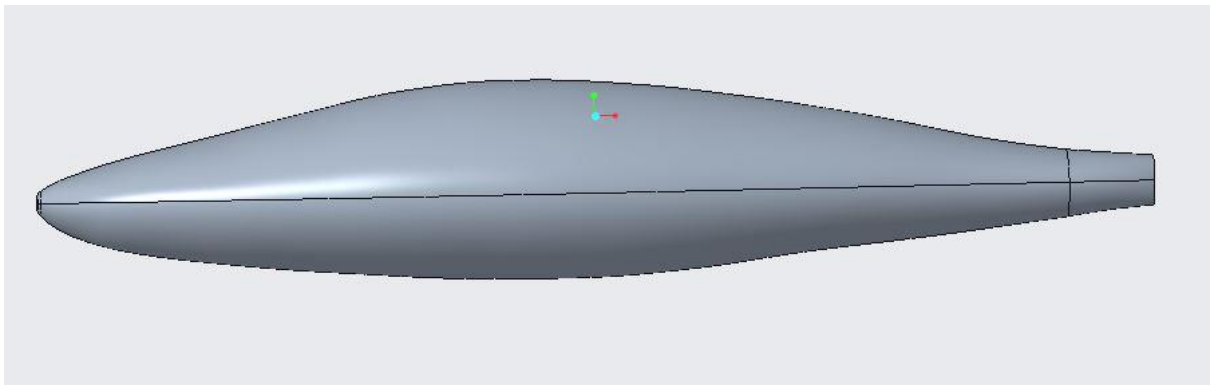
Figure 49: The proposed Hvaldimir 2.0.

During the development of Hvaldimir, the advanced geometry proved to be challenging to model, as well as producing some very interesting mesh shapes. By utilizing the methods used in [30], a mathematical model can be used to produce a more streamlined foil-like shape for better hydrodynamic properties.

Initially, the scope of the task was broader than the result, as the original goal was to improve on the Hugin drone using the original hull as a starting point. Due to communication issues with FFI and Kongsberg, the Hugin model could not be acquired, so the reference model had to be created using measurements from pictures and older models. This resulted in different volumes and vetted surfaces between the drones, even though it would be optimal to have these as similar as possible.

5. Conclusion

Comparing the flow around the drones makes it obvious that the reference model has an advantageous design. Lack of abrupt changes along the body reduces high pressure areas besides the nose, which reduces unnecessary areas of increased drag. If this is changed on Hvaldimir the design could be improved and the drag could be further reduced.

When comparing the turbulence induced by the designs there is a clear advantage in creating a streamlined body. This seems to be the biggest factor for decreasing drag affecting the drones. The area of low pressure behind the drones creates a component of the drag which "pulls" the drone backwards. Since the low-pressure area is proportional with increase in turbulence, a design objective for drones should be reduction in turbulence by the creation of a streamlined body.

The results produced by the tests through Section 3 proves that the performance of the two drones was in most cases similar, with Hvaldimir performing somewhat worse than the reference model. Even though the drag coefficient proved to be lower for Hvaldimir, the overall drag force turned out to be higher, thus making Hvaldimir spend more energy per distance travelled in the water. This is mainly due to Hvaldimir having a larger projected area and wetted surface, thus causing a lower drag coefficient but more drag force than the reference model.

More research is needed in order to determine the exact reason for the performance differences between the hulls in this thesis. However, one can conclude that both drones perform a lot better than the cylindrical model with a highly turbulent wake. The results may indicate that there is no decisive difference in drag force and thus effectiveness when designing streamlined AUV hulls, and that economical and practical implications such as construction complexity and equipment arrangement may be conclusive objectives then producing an AUV.

Access to a towing tank would confirm the accuracy of the results achieved in the CFD analysis, as different versions of the ANSYS software has yielded somewhat different drag values. The drag force differences between the full version is 100% higher than the student version, a significant variation. This large increase most likely comes from the fact that the full version software has a higher poly count and a more accurate mesh, thus being able to simulate friction and drag with higher precision.

As there was a minimal amount of earlier research in the same field, expanding the knowledge of biological hull shapes turned out to be an interesting task. It is recommended that other bachelor groups continue working on this problem by experimenting with other shapes and dimensions, or by adding new equipment such as sensors and antennas to the drone, as this was one of the problems specifically requested by one of the thesis initiators.

6. Bibliography

[1]   T. Liu, Y. Liu, L. Zhang, H. Zhang, Z. Wu, and Y. Wang, "Hydrodynamic Shape Genealogy for Teardrop-shaped Autonomous Underwater Vehicles," ed: Key Laboratory of Mechanism Theory and Equipment Design of Ministry of Education, School of Mechanical Engineering, Tianjin University   2017.

[2]   Kongsberg. "Using the Hugin AUV for Fishery Research Purposes." (accessed 19.03, 2020).

[3]   C. Eriksen *et al.*, "Seaglider: A long-range autonomous underwater vehicle for oceanographic research," *Oceanic Engineering, IEEE Journal of,* vol. 26, pp. 424-436, 11/01 2001, doi: 10.1109/48.972073.

[4]   Equinor. "The machines are coming!" (accessed 19.03, 2020).

[5]   Kongsberg, "HUGIN Superior Autonomous Underwater Vehicle (AUV)," H. S. a. u. vehicle, Ed., ed. https://www.naval-technology.com/projects/hugin-superior-auv/: Kongsberg

[6]   Kongsberg, "KONGSBERG'S SEAGLIDER DIVISION TRANSFERRED TO HYDROID," ed. https://sea-technology.com/hydroid-seaglider, 2019.

[7]   Equinor, "Eelume," ed. https://www.equinor.com/en/magazine/here-are-six-of-the-coolest-offshore-robots.html.

[8]   A. B. Phillips, S. R. Turnock, and M. Furlong, "The Use of Computational Fluid Dynamics to Aid Cost-Effective Hydrodynamic Design of Autonomous Underwater Vehicles," vol. 224, no. 4, pp. 239-254, 2010, doi: https://doi.org/10.1243/14750902JEME199.

[9]   D. F. Myring, "A Theoretical Study of the Effects of Body Shape and Mach Number on the Drag of Bodies of Revolution in Subcritical Axisymmetric Flow," ed, 1981.

[10]   G. R. Carrasco, A. Viedma, and A. C. Toledo, "Coefficient estimation in the dynamic equations for motion of an AUV," Departamento de Technologia Naval, Universidad Politecnica de Cartagena (UPCT)   SIXTH INTERNATIONAL WORKSHOP ON MARINE TECHNOLOGY, Martech 2015, 2015.

[11]   T. Gao, Y. Wang, Y. Pang, and J. Cao, "Hull shape optimization for autonomous underwater vehicles using CFD," *Engineering Applications of Computational Fluid Mechanics,* vol. 10, no. 1, pp. 599-607, 2016, doi: 10.1080/19942060.2016.1224735.

[12]   N. A. Cruz and A. C. Matos, "The MARES AUV, a Modular Autonomous Robot for Environmental Sampling," Faculdade de Engenharia, Universidade do Porto, 2008.

[13]   M. W. Glier, J. Tsenn, J. S. Linsey, and D. A. McAdams, "Methods for Supporting Bioinspired Design," pp. 737-744, 2011, doi: https://doi.org/10.1115/IMECE2011-63247.

[14]   D. Weihs, "A hydrodynamical analysis of fish turning manoeuvres," 182, Department of Applied Mathematics and Theoretical Physics, University of Cambridge, Cambridge, England, 1972.

[15]   B. Dean and B. Bhushan, "Shark-Skin Surfaces for Fluid-Drag Reduction in Turbulent Flow: A Review," *Philosophical transactions. Series A, Mathematical, physical, and engineering sciences,* vol. 368, pp. 4775-806, 10/28 2010, doi: 10.1098/rsta.2010.0201.

[16]   Creo. "Creo® Installation and Administration Guide."
         https://support.ptc.com/WCMS/files/171806/en/creo4_m040_install.pdf (accessed
         19.03.2020).

[17]   K. Kuiper. "Streamlining." https://www.britannica.com/science/streamlining (accessed
         05.02.2020).

[18]   G. Aquarium, "Blacktip Reef Shark," https://www.georgiaaquarium.org/animal/blacktip-reef-
         shark/.

[19]   Y. A. Cengel and J. M. Cimbala, *Fluid Mechanics Fundementals and Applications*, 4th ed.
         Library of Congress Cataloging-in-Publication Data: McGraw-Hill Education, 2017.

[20]   J. D. J. Anderson, *Fundamentals of Aerodynamics*, 5th ed. McGraw-Hill Education, 2010.

[21]   V. Bertram, "Resistance and Propulsion," 2012. [Online]. Available:
         https://www.sciencedirect.com/topics/engineering/frictional-resistance.

[22]   H. Walderhaug, "Motstand, framdrift, styring," ed. Marine Technology Centre, Trondheim,
         Norway: Department of Marine Technology, Norwegian Institute of Technology, 1992.

[23]   N. Hall. "Boundary Layer." NASA Official. https://www.grc.nasa.gov/WWW/K-
         12/airplane/boundlay.html (accessed 05.02.2020).

[24]   N. Hall. "Navier-Stokes Equations." NASA Official. https://www.grc.nasa.gov/WWW/k-
         12/airplane/nseqs.html (accessed 07.02.2020).

[25]   J. P. Ellenberger, *Chapter 4 - Piping and Pipeline Sizing, Friction Losses, and Flow
         Calulations*. 2014.

[26]   B. E. Rapp, "Microfluidics: Modelling, Mechanics and Mathematics," ed, 2017.

[27]   N. Hall, "The Drag Equation," NASA Official. https://www.grc.nasa.gov/www/k-
         12/airplane/drageq.html (accessed 10.02.2020).

[28]   I. ANASYS. "ANSYS CFX-Pre User's Guide."
         http://read.pudn.com/downloads500/ebook/2077964/cfx_pre.pdf (accessed 27.04. 2020).

[29]   P. Jagadeesh and K. Murali, "Application of low-Re turbulence models for flow simulations
         past underwater vehicle hull forms," ed. Journal of Naval Architecture and Marine
         Engineering, 2005.

[30]   A. Muratoglu, "Hydrodynamic analysis of shark body hydrofoil using CFD methods,"
         International Journal of Engineering Research and Development, no. 227-237, 2019.
         [Online]. Available:
         https://www.researchgate.net/publication/331145186_Hydrodynamic_analysis_of_shark_body
         _hydrofoil_using_CFD_methods.